PAPER

Blow-up dynamics and spectral property in the L^2-critical nonlinear Schrödinger equation in high dimensions

IOP Publishing | London Mathematical Society Nonlinearity

Nonlinearity **31** (2018) 4354–4392 https://doi.org/10.1088/1361-6544/aacc41

Blow-up dynamics and spectral property in the L^2-critical nonlinear Schrödinger equation in high dimensions

Kai Yang, Svetlana Roudenko and Yanxiang Zhao

Department of Mathematics, George Washington University, Washington, DC, United States of America

E-mail: svetlanamath@gmail.com

Received 31 December 2017, revised 16 May 2018
Accepted for publication 13 June 2018
Published 7 August 2018

Recommended by Dr Claude Le Bris

Abstract

We study stable blow-up dynamics in the L^2-critical nonlinear Schrödinger (NLS) equation in high dimensions. First, we show that in dimensions $d = 4$ to $d = 12$ generic blow-up behavior confirms the *log–log* regime in our numerical simulations under the radially symmetric assumption, and asymptotic analysis, including the log–log rate and the convergence of the blow-up profiles to the rescaled ground state; this matches the description of the stable blow-up regime in the 2D cubic NLS equation.

Next, we address the question of rigorous justification of the *log–log* dynamics in higher dimensions ($d \geqslant 5$), at least for the initial data with the mass slightly larger than the mass of the ground state, for which the spectral conjecture has yet to be proved, see Merle and Raphaël (2005 *Ann. Math.* **161** 157–222) and Fibich *et al* (2006 *Physica* D **220** 1–13). We give a numerically-assisted proof of the spectral property for the dimensions from $d = 5$ to $d = 12$, and a modification of it in dimensions $2 \leqslant d \leqslant 12$. This, combined with previous results of Merle–Raphaël, proves the *log–log* stable blow-up dynamics in dimensions $d \leqslant 10$ and radially stable for $d \leqslant 12$.

Keywords: stable blow-up, log–log blow-up, nonlinear Schrödinger equation, spectral property, dynamic rescaling method
Mathematics Subject Classification numbers: Primary: 35Q55, 35Q40; secondary: 35P30

(Some figures may appear in colour only in the online journal)

1. Introduction

We consider the Cauchy problem of the L^2-critical nonlinear Schrödinger (NLS) equation:

$$\begin{cases} \mathrm{i}u_t + \Delta u + |u|^{\frac{4}{d}}u = 0, & (t,x) \in \mathbb{R}\times\mathbb{R}^d \\ u(x,0) = u_0 \in H^1(\mathbb{R}^d). \end{cases} \tag{1.1}$$

The local well-posedness of the equation (1.1) in H^1 is given by Ginibre and Velo in [14], see also [7]. It shows that for $u_0 \in H^1(\mathbb{R}^d)$, there exists $0 < T \leqslant \infty$ such that there is a unique solution $u(t) \in \mathbb{C}([0,T), H^1(\mathbb{R}^d))$. We say the solution exists globally in time if $T = \infty$, and the solution blows up in finite time if $T < \infty$ and $\limsup_{t \nearrow T} \|\nabla u(t)\|_{L^2} = \infty$.

During their lifespan, the solutions $u(x,t)$ of the Cauchy problem (1.1) satisfy the following conservation laws

$$\text{Mass}: \quad M(u(x,t)) \overset{\text{def}}{=} \int |u(x,t)|^2 \,\mathrm{d}x = \int |u_0(x)|^2 \,\mathrm{d}x, \tag{1.2}$$

$$\text{Energy}: \quad E(u(x,t)) \overset{\text{def}}{=} \frac{1}{2}\int |\nabla u(x,t)|^2 \,\mathrm{d}x - \frac{1}{2+\frac{4}{d}}\int |u(x,t)|^{2+\frac{4}{d}} \,\mathrm{d}x = E(u_0), \tag{1.3}$$

$$\text{Momentum}: \quad P(u(x,t)) \overset{\text{def}}{=} \mathrm{Im}\left(\int \nabla u(x,t)\bar{u}(x,t)\,\mathrm{d}x\right) = \mathrm{Im}\left(\int \nabla u_0(x)\bar{u}_0(x)\,\mathrm{d}x\right). \tag{1.4}$$

Substituting $u(t,x) = \mathrm{e}^{\mathrm{i}t}Q(x)$ into (1.1), we obtain a special class of periodic solutions with Q solving

$$-\Delta Q + Q - |Q|^{\frac{4}{d}}Q = 0. \tag{1.5}$$

The equation (1.5) exhibits many solutions, even when restricted to those that are smooth and vanishing-at-infinity. In this work we are only interested in real positive solutions. The existence and uniqueness of a real, positive, vanishing-at-infinity solution of (1.5) are obtained in [4] and [22], and this solution is referred to as the ground state solution, which we also denote by Q. Note that the ground state solution is radially symmetric $Q = Q(r)$, moreover, it is exponentially decaying at infinity, [4]. For the purpose of this paper, we will simply say $Q \in H^1(\mathbb{R}^d)$. In the dimension $d = 1$, the ground state solution of (1.5) is explicit

$$Q(x) = 3^{1/4}\mathrm{sech}^{1/2}(2x). \tag{1.6}$$

While in dimensions $d \geqslant 2$, the ground state is not explicit, its properties are known, and various numerical methods (e.g. renormalization method or shooting method, see, for example, the monograph [9] and reference therein) produce the ground state Q numerically.

The importance of the ground state comes into play when one wants to understand the long time behavior of solutions. In 1983, Weinstein [51] showed that solutions exist globally in time if $\|u_0\|_{L^2} < \|Q\|_{L^2}$. By convexity arguments on a finite variance, it is known that solutions blow up in finite time if $E[u_0] < 0$, see [49, 55] or [15]. Thus, solutions with $\|u_0\|_{L^2} \geqslant \|Q\|_{L^2}$ may blow up in finite time. Moreover, the minimal mass blow-up solutions happen exactly at the threshold $\|u_0\|_{L^2} = \|Q\|_{L^2}$, and the classification of all minimal mass blow-up solutions was done by Merle in [31] (radial) and [32] (general case). We note that all minimal mass blow-up solutions are unstable. In this paper we are interested in stable blow-up dynamics, thus, we consider the initial data with the mass above the mass of the ground state Q.

Investigations of the stable blow-up dynamics for the NLS equation (mainly in the 2D case, i.e. cubic nonlinearity) go back to 1970s (for example, [5, 16, 45, 46]). In 1986, McLaughlin, Papanicolaou, Sulem and Sulem in [30] (see also [44]) showed that the rate of stable blow-up should be coming from scaling and equivalent to $(T-t)^{-\frac{1}{2}}$ by applying the dynamic rescaling method. Previously, Talanov and collaborators (1978), Wood (1984) and Rypdal and Rasmussen (1986) suggested a form of $(|\ln(T-t)|/(T-t))^{\frac{1}{2}}$ from a different approach, see [41, 50, 53]. Then, Landman, Papanicolaou, Sulem, and Sulem in [24] (also LeMesurier, Papanicolaou, Sulem and Sulem in [26]) as well as Fraiman [13], and others (see [8, 21, 23, 28]; for a more complete reference list on this subject refer to [44]) concluded from asymptotic analysis, incorporating numerical simulations, that the rate of blow-up is of the form $\left(\frac{\ln|\ln(T-t)|}{(T-t)}\right)^{\frac{1}{2}}$, which is now referred to as the 'log–log' law. Later in 1990, Landman, Papanicolaou, Sulem, Sulem and Wang in [25] concluded that this log–log rate is a stable blow-up rate in 2D by simulating the blow-up dynamics without radial symmetry assumption. Note that numerical tracking of the log–log correction is extremely difficult as it is reached only at exceedingly huge focusing levels (of orders $\sim$200), for example, see [12], and thus, asymptotic analysis was used in [24, 26] to obtain the log–log correction. An alternative approach was developed by Akrivis, Dougalis, Karakashian and McKinney in 1993 and 1997, see [1, 2], where very accurate computations of the solution were performed using an adaptive Galerkin finite element method. The computed solution was then tested against several theoretical predictions for the functional form of the correction, and the log–log law was selected for the far asymptotic regime as the best fitting. Recently, there have been (very refined and to exorbitantly high focusing levels) numerical studies beyond the leading order of the stable blow-up dynamics, see Lushnikov, Dyachenko and Vladimirova [27], where the authors obtained higher order correction terms in the log–log blow-up rate.

While it was important to investigate the stable blow-up dynamics numerically and heuristically, the rigorous analytical description started appearing only at the turn of this century. Galina Perelman in 2001, see [37] (also [38]), made a rigorous construction of the 'log–log' blow-up solutions in the 1D case (i.e. for the quintic NLS equation $\mathrm{i}u_t + u_{xx} + |u|^4 u = 0$). As it was the first analytical proof of the 'log–log' blow-up, it opened possibilities to study blow-up solutions rigorously. In the series of papers [33–35], [36, 39], Merle and Raphaël did a systematic study of the generic blow-up, considering initial data slightly above the ground state mass and with negative energy, and obtained a detailed description of the dynamics, in particular, the convergence of the blow-up profiles to the self-similarly rescaled Q and the blow-up rate $\left(\frac{\ln|\ln(T-t)|}{(T-t)}\right)^{\frac{1}{2}}$. This description was proved for any dimension, provided the so-called 'spectral property' holds true (see the actual statement below). This spectral property was proved rigorously in the one dimensional case in [33], since the ground state Q is explicit in 1D (1.6) and the spectral property could be deduced from some known properties of the second-order differential operators [47]. For the dimensions $d = 2, 3, 4$, Fibich, Merle and Raphaël gave a numerically-assisted proof of the spectral property, using the numerical representation of Q, see [10] and [11]. For $d \geqslant 6$, the authors in [10] indicated that the spectral property is indecisive (via their approach), furthermore, there was no direct numerical simulation of the blow-up solutions in higher dimensions, even under the radial symmetry assumption (all prior L^2-critical NLS numerical simulations were in 2D), as it could have been a computationally difficult task at that time. Investigating stable blow-up regime in higher dimensions is the goal of this work.

In this paper, we first show that in higher dimensions, $4 \leqslant d \leqslant 12$, a generic self-similar blow-up dynamics is also described by the 'log–log' law, i.e. our numerical simulations show

that the blow-up profiles converge to the self-similar ground state, furthermore, we obtain the log–log blow-up rate via derivation as in [44, section 8] and matching refinement adapted from [1]. As we only numerically simulate the radial case, we conclude in this first part that this log–log blow-up dynamics is radially stable. Secondly, we give a proof of the spectral property for $d = 5, ..., 12$, which completes the rigorous proof of the stable blow-up dynamics for the dimensions $d \leqslant 12$ for the initial data with negative energy and mass slightly above the mass of the ground state.

For consistency, in what follows, we adopt the notation from [10] and [44]: denote by B_α a neighborhood of H^1 functions with the L^2 norm slightly above the mass of the ground state Q, i.e. $B_\alpha = \left\{ f \in H^1(\mathbb{R}^d) : \int Q^2 < \int |f|^2 < \int Q^2 + \alpha \right\}$; the variable $x = (x_i)_{1 \leqslant i \leqslant d}$ is used as the space variable, $r = |x|$ stands for the radial coordinate and the radial derivative $\partial_r f(r)$ we typically write as f_r; we also denote H^1_r as the space of radial functions in H^1, and $\langle\ ,\ \rangle$ as the standard inner product on L^2. We define the scaling symmetry generator acting on Q by

$$Q_1 = \frac{d}{2} Q + x \cdot \nabla Q, \quad \text{and also define} \quad Q_2 = \frac{d}{2} Q_1 + x \cdot \nabla Q_1. \tag{1.7}$$

Spectral property 1.([10, 29]). Let $d \geqslant 1$. Consider the two real Schrödinger operators

$$L_1 = -\Delta + V_1 \quad \text{and} \quad L_2 = -\Delta + V_2, \tag{1.8}$$

where

$$V_1(r) = \frac{2}{d} \left(\frac{4}{d} + 1 \right) Q^{\frac{4}{d}-1} r Q_r, \tag{1.9}$$

$$V_2(r) = \frac{2}{d} Q^{\frac{4}{d}-1} r Q_r, \tag{1.10}$$

and the real-valued quadratic form for $u = f + ig \in H^1(\mathbb{R}^d)$ is defined as

$$B(u,u) = B_1(f,f) + B_2(g,g) \tag{1.11}$$

$$= \langle L_1 f, f \rangle + \langle L_2 g, g \rangle. \tag{1.12}$$

Then there exists a universal constant $\delta_0 > 0$ such that for any $u \in H^1(\mathbb{R}^d)$, if the following orthogonal conditions hold

$$\langle f, Q \rangle = \langle f, Q_1 \rangle = \langle f, x_i\, Q \rangle_{1 \leqslant i \leqslant d} = 0, \tag{1.13}$$

$$\langle Q_1, g \rangle = \langle Q_2, g \rangle = \langle \partial_{x_i} Q, g \rangle_{1 \leqslant i \leqslant d} = 0, \tag{1.14}$$

then $B(u,u) > 0$, or more precisely,

$$B(u,u) \geqslant \delta_0 \left(\int |\nabla u|^2 + |u|^2 \mathrm{e}^{-|x|} \right). \tag{1.15}$$

We note that the commutator-type formulas hold for the operators L_1 and L_2, which was observed in [33],

$$L_1 f = \frac{1}{2} \left[L_+(f_1) - (L_+ f)_1 \right] \quad \text{and} \quad L_2 g = \frac{1}{2} \left[L_-(g_1) - (L_- g)_1 \right],$$

where L_+ and L_- are the standard linearized operators obtained from the linearization of solutions around the ground state Q:

$$L_+ = -\Delta + 1 - \left(1 + \frac{4}{d}\right) Q^{\frac{4}{d}}, \tag{1.16}$$

$$L_- = -\Delta + 1 - Q^{\frac{4}{d}}. \tag{1.17}$$

We mention that the choice of the orthogonal conditions (1.13) and (1.14) in the above spectral property 1 comes from the generalized null space of the matrix operator $\mathcal{L} = \begin{bmatrix} 0 & L_- \\ -L_+ & 0 \end{bmatrix}$ (see e.g. Weinstein [52], Buslaev–Perelman [6]).

Our first result is the following:

Theorem 1.1. *The spectral property 1 holds true in dimensions from $d = 5$ to $d = 10$. The spectral property 1 holds true in the radial case for dimensions $d = 11$ and $d = 12$.*

We next modify the statement of the spectral property 1.

Spectral property 2. Let $d \geqslant 2$ and assume the same set up as in the spectral property 1, except replace the orthogonal conditions (1.14) by

$$\langle Q, g\rangle = \langle \partial_{x_i} Q, g\rangle_{1\leqslant i\leqslant d} = 0. \tag{1.18}$$

Then $B(u,u) > 0$, or (1.15) is true (i.e. the same conclusion as in the spectral property 1 holds).

Our second result is about the modified spectral property.

Theorem 1.2. *The spectral property 2 holds true in dimensions from $d = 2$ to $d = 10$. The spectral property 2 holds true in the radial case for dimensions $d = 11$ and $d = 12$.*

The spectral property 1 added to the work of Merle–Raphaël [33–36], and Fibich–Merle–Raphaël [10], now fully completes the proof of the stable blow-up dynamics in dimensions $d \leqslant 10$, and radially stable in $d \leqslant 12$ with the description of various dynamical features (profile, rate, phase, control of the remainder, etc; we note that the bounded control in the external region is given in [18]). For completeness of this introduction, we provide a concise statement of the stable blow-up dynamics below.

Theorem 1.3 (Stable blow-up dynamics of (1.1)). *Assume the spectral property holds true, which is now proved for $d \leqslant 10$ and in the radial case for $d = 11, 12$.*

There exist universal constants $\alpha > 0$ and $C > 0$ such that the following holds true. For $u_0 \in B_\alpha$, let $u(t)$ be the corresponding H^1 solution to (1.1) on $[0, T)$, the interval of the maximal in forward time existence of u.

(i) Description of the singularity: Assume that $u(t)$ blows up in finite time, i.e. $0 < T < \infty$. Then there exist parameters $(\lambda(t), x(t), \gamma(t)) \in \mathbb{R} \times \mathbb{R}^d \times \mathbb{R}$ and asymptotic profile $u^* \in L^2$ such that

$$u(t) - \frac{1}{\lambda(t)^{\frac{d}{2}}} Q\left(\frac{x - x(t)}{\lambda(t)}\right) \mathrm{e}^{\mathrm{i}\gamma(t)} \to u^* \quad \text{in } L^2(\mathbb{R}^d) \quad \text{as } t \to T.$$

Moreover, the blow-up point is finite in the sense that

$$x(t) \to x(T) \in \mathbb{R}^d \quad as \ t \to T.$$

(ii) Estimates on the blow-up speed: for t close enough to T, either

$$\lim_{t\to T} \frac{|\nabla u(t)|_{L^2}}{|\nabla Q|_{L^2}} \left(\frac{T-t}{\ln|\ln(T-t)|}\right)^{\frac{1}{2}} = \frac{1}{\sqrt{2\pi}}, \tag{1.19}$$

or

$$|\nabla u(t)|_{L^2} \geqslant \frac{C(u_0)}{T-t}.$$

The equation (1.19) is referred to as the 'log–log' blow-up rate.

(iii) Sufficient condition for 'log–log' blow-up[1]*: If $E(u_0) < 0$ and $\int Q^2 < \int |u_0|^2 < \int Q^2 + \alpha$, then $u(t)$ blows up in finite time with the 'log–log' rate (1.19). More generally, the set of initial data $u_0 \in B_\alpha$ such that the corresponding solution $u(t)$ to (1.1) blows up in finite time $0 < t < \infty$ with the 'log–log' speed (1.19) is open in H^1.*

Remark 1.4. Our numerical simulations show that for the initial data u_0 of the Gaussian-type, $u_0 \sim A\mathrm{e}^{-r^2}$, or of the ground state-type, $u_0 \sim A\,\mathrm{e}^{-r}$, the parameter α in theorem 1.3 (iii) can be taken very large, i.e. $\alpha = \infty$.

This paper consists of two parts. In the first part, section 2, we show the results from the direct numerical simulations of solutions in the L^2-critical NLS equation in dimensions $4 \leqslant d \leqslant 12$ by the dynamic rescaling method for the radially symmetric data. This shows that the blow-up rate is $(T-t)^{-\frac{1}{2}}$, possibly with some correction terms. Applying the arguments from [24] and [26], we show that the correction term indeed exists, which can be obtained via asymptotic analysis $q(t) \approx \left((2\pi)/\ln\ln\frac{1}{|T-t|}\right)^{\frac{1}{2}}$, and to further confirm it, we apply the approach from [1] to fit the solution with various functional forms. This leads us to the conclusion that at least for the radial data in the dimensions $d = 4, ..., 12$, the 'log–log' blow-up dynamics is generic and stable, see section 2.2 for details. In the second part of the paper, section 3, we revisit the spectral property 1 and give a numerically-assisted proof of it for dimensions up to $d = 10$ (general case), and for the radially symmetric case for $d = 11$ and $d = 12$; we then also establish the spectral property 2. In appendices, we provide the rest of the numerical simulations in dimensions $d = 6, ..., 12$ (the simulations for $d = 4, 5$ are in section 2.2); we discuss the artificial boundary conditions; we describe a new approach to compute the potentials $V_{1,2}$ in high dimensions; and also provide comparison with previous results from [10] of the spectral property 1 for $d = 2, 3, 4$.

2. Numerical simulations of the solutions

In this section, we first review the dynamic rescaling method which is applied in our numerical simulations. Then, we present our numerical results. These numerical findings, combined with the analysis in [24] and [26], adapted to our setting, shows the 'log–log' blow-up rate.

2.1. Dynamic rescaling method

We use the dynamic rescaling method (see [30] and [44]) for simulating the blow-up solutions of the equation (1.1). The key idea of this method is to appropriately rescale the equation (1.1)

[1] A more general description is $E(u_0) < \frac{1}{2}\frac{[P(u_0)]^2}{M(u_0)}$, see [33, 34].

in both time and space variables. Then solutions for the rescaled equation exist globally in time. We restrict our numerical simulations under the radially symmetric assumption. Letting $\sigma = \frac{2}{d}$, where d is the dimension, we set

$$u(r,t) = \frac{1}{L(t)^{\frac{1}{\sigma}}} v(\xi,\tau), \quad \text{where} \quad \xi = \frac{r}{L(t)}, \quad \tau = \int_0^t \frac{\mathrm{d}s}{L^2(s)}. \tag{2.1}$$

Given a prescribed value $L(0)$ (e.g. $L(0) = 1$), we obtain the initial condition $v_0(\xi) = L(0)^{\frac{1}{\sigma}} u_0(r)$. Then the equation (1.1) becomes

$$iv_\tau + ia(\tau)\left(\xi v_\xi + \frac{v}{\sigma}\right) + \Delta_\xi v + |v|^{2\sigma} v = 0, \tag{2.2}$$

with boundary conditions

$$v_\xi(0) = 0, \qquad v(\infty) = 0, \tag{2.3}$$

where

$$a = -L\frac{\mathrm{d}L}{\mathrm{d}t} = -\frac{\mathrm{d}\ln L}{\mathrm{d}\tau}. \tag{2.4}$$

There are various choices for tracking the parameter $L(t)$. The first choice is the following: since we want to bound $\|\nabla u(t)\|_{L^2}$ as $t \to T$, we choose the parameter $L(t)$ such that the value of $\|\nabla_\xi v(\tau)\|_{L^2}$ in the rescaled equation (2.2) remains constant in time, i.e.

$$L(t) = \left(\frac{\|\nabla_\xi v_0\|_{L^2}}{\|\nabla u(t)\|_{L^2}}\right)^{2/p}, \qquad p = 2 + \frac{2}{\sigma} - d. \tag{2.5}$$

Then, $a(\tau)$ is, consequently,

$$a(\tau) = -\frac{2}{p\|v_0\|_{L^2}^2} \int_0^\infty |v|^{2\sigma} \mathrm{Im}\,(\bar{v}\Delta v)\, \xi^{d-1} \mathrm{d}\xi. \tag{2.6}$$

An alternative choice for the $L(t)$ is to fix the L^∞ norm of v such that $\|v\|_{L^\infty}$ remains constant (see [21, 26] for such a choice), thus, set

$$L(t) = \left(\frac{v_0(0)}{\|u(t)\|_{L^\infty}}\right)^\sigma, \tag{2.7}$$

and hence, $a(\tau)$ rewrites as

$$a(\tau) = -\frac{\sigma}{|v_0(0)|^2} \mathrm{Im}\,(\bar{v}\Delta_\xi v)\,|_{(0,\tau)}. \tag{2.8}$$

The above two choices are typical rescalings, for example, see [30] and [44].

To discuss our numerical scheme, we note that the equation (2.2) is of the form

$$iv_\tau + \Delta_\xi v + \mathcal{N}(v) = 0, \quad \tau \in [0,\infty), \quad \xi \in [0,\infty), \tag{2.9}$$

where

$$\mathcal{N}(v) = \mathrm{i}a(\tau)\left(\xi v_\xi + \frac{v}{\sigma}\right) + |v|^{2\sigma} v.$$

Before we discretize the space variable ξ, we need to map the spatial domain $[0,\infty)$ onto $[-1,1)$, since $\xi \in [0,\infty)$. One possible way to do that is to set $\xi = \kappa\frac{1+z}{1-z}$, where κ is a constant indicating the half number of the collocation points assigned on the interval $[0,\kappa]$, and z is the Chebyshev–Gauss–Lobatto collocation points on the interval $[-1,1]$, for instance see [43] and

[48]. Because of the homogeneous Dirichlet boundary condition $v(\infty) = 0$ on the right, we remove the last Chebyshev point, and, consequently, delete the last row and the last column of the matrix $\mathbf{M}$ in (2.12). This is similar with the singular behavior at $x \to \infty$ in [3] in which the authors impose No boundary condition at $x \to \infty$. The Laplacian operator can be discretized by Chebyshev–Gauss–Lobatto differentiation (for details refer to [43] and [48]). We denote the discretized Laplacian with $N + 1$ collocation points by Δ_N. Note that

$$\Delta_\xi v = v_{\xi\xi} + \frac{d-1}{\xi} v_\xi.$$

The singularity at $\xi = 0$ is eliminated by applying the L'Hôspital's rule:

$$\lim_{\xi \to 0} \frac{d-1}{\xi} v_\xi = (d-1) v_{\xi\xi}.$$

We use the following notation for v: let $v^{(m)}$ be the discretized v at the time $\tau = m \cdot \delta\tau$, where $\delta\tau$ is the time step and m is the iteration. The time evolution of (2.9) can be approximated by the second order Crank–Nicolson–Adam–Bashforth method:

$$i\frac{v^{(m+1)} - v^{(m)}}{\delta\tau} + \frac{1}{2}\left(\Delta_N v^{(m+1)} + \Delta_N v^{(m)}\right) + \frac{1}{2}\left(3\mathcal{N}(v^{(m)}) - \mathcal{N}(v^{(m-1)})\right) = 0. \tag{2.10}$$

We reorganize (2.10) as

$$\left(\frac{\mathrm{i}}{\delta\tau} + \frac{1}{2}\Delta_N\right) v^{(m+1)} = \left(\frac{\mathrm{i}}{\delta\tau} - \frac{1}{2}\Delta_N\right) v^{(m)} - \frac{1}{2}\left(3\mathcal{N}(v^{(m)}) - \mathcal{N}(v^{(m-1)})\right), \tag{2.11}$$

which is equivalent to

$$\mathbf{M} v^{(m+1)} = F(v^{(m)}, v^{(m-1)}). \tag{2.12}$$

Therefore, the time step is updated by

$$v^{(m+1)} = \mathbf{M}^{-1} F(v^{(m)}, v^{(m-1)}). \tag{2.13}$$

The inverse of the matrix $\mathbf{M}$ can be calculated only once in the beginning, since $\mathbf{M} = \left(\frac{\mathrm{i}}{\mathrm{d}\tau} + \frac{1}{2}\Delta_N\right)$, which stays the same.

The boundary conditions (2.3) are imposed similar to [30, 48] and [43] as follows: For the homogeneous Neumann boundary condition ($v_\xi(0) = 0$) on the left, we substitute the first row of the matrix $\mathbf{M}$ by the first row of the first order Chebyshev differential matrix, and change the first element of the vector F to 0. Because of the homogeneous Dirichlet boundary condition $v(\infty) = 0$ on the right, we delete the last row and column of $\mathbf{M}$ as well as the last element of the vector F.

An alternative method is to use predictor-corrector method similar to [9],

$$i\frac{v_{\text{pred}}^{(m+1)} - v^{(m)}}{\delta\tau} + \frac{1}{2}\left(\Delta_N v_{\text{pred}}^{(m+1)} + \Delta_N v^{(m)}\right) + \frac{1}{2}\left(3\mathcal{N}(v^{(m)}) - \mathcal{N}(v^{m-1})\right) = 0, \ \text{(P)} \tag{2.14}$$

$$i\frac{v^{(m+1)} - v^{(m)}}{\delta\tau} + \frac{1}{2}\left(\Delta_N v^{(m+1)} + \Delta_N v^{(m)}\right) + \frac{1}{2}\left(\mathcal{N}(v_{\text{pred}}^{(m+1)}) + \mathcal{N}(v^{(m-1)})\right) = 0. \ \text{(C)}. \tag{2.15}$$

The above two schemes lead to the similar results. Numerical test suggests that the scheme (2.14) and (2.15) is slightly more accurate than the scheme (2.10), though it is still second

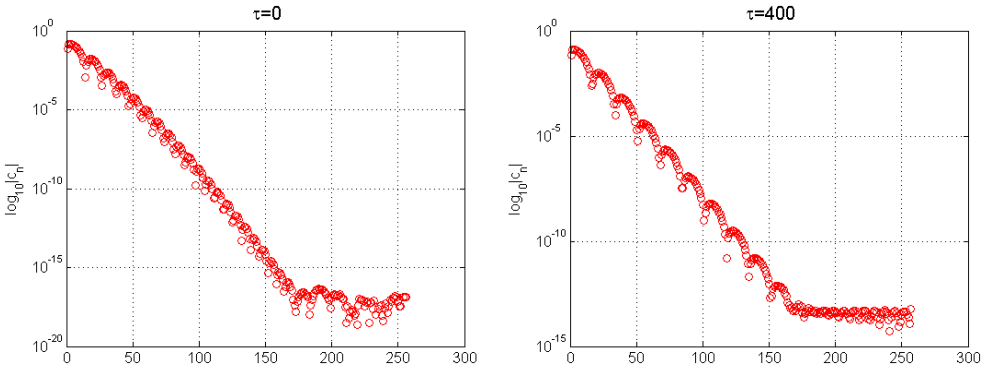

Figure 1. The Chebyshev coefficients for the solution v in the case $d = 4$ at time $\tau = 0$ (left) and $\tau = 400$ (right). One can see the value $|c_n|$ reaches the machine's accuracy around $N_0 = 170$.

order in time and doubles the computational time. We mainly use the 'predictor-corrector' scheme (2.14) and (2.15) in our simulation.

Note that it is sufficient to use $N = 256$ collocation points. For any sufficiently smooth function f over $[-1, 1]$, $f(x)$ can be expanded by the Chebyshev polynomials

$$f(x) = \sum_{n=0}^{\infty} c_n T_n(x), \quad c_n \to \infty \text{ as } n \to \infty. \tag{2.16}$$

Therefore, we choose a number N_0 such that the coefficients c_n are sufficiently small (generally reaches the machine's accuracy 10^{-16}) for $n \geqslant N_0$. Figure 1 shows the Chebyshev coefficients $|c_n|$ of the numerical solution v in the case $d = 4$ at different times $\tau = 0$ and $\tau = 400$. One can see that $|c_n|$ reaches the order 10^{-12} around $N_0 = 128$, and reaches the machine's accuracy around $N_0 = 170$. Hence, it is sufficient to choose any $N > N_0$. Since the Chebyshev transform can be processed by the fast Fourier transform (e.g. [43, 48] and [3]), we choose $N = 256$, a power of 2. Similar study for the decaying behavior of the Chebyshev coefficients c_n for multidomain spectral method for Schrödinger equation can be found in [3].

We choose $\kappa = 256$ and $\mathrm{d}\tau = 2 \times 10^{-3}$. We set $v_0(0) = 1$ and we choose to fix the value $\|v(\tau)\|_\infty \equiv 1$ in time τ. Then the parameter $L(t)$ becomes $L(t) = (1/\|u(t)\|_{L^\infty})^{\sigma}$, see [26]. We decided not to fix the value of $\|\nabla v(\tau)\|_{L^2}$ to be constant in high dimensions since it involves integrating $\int_0^\infty ... \xi^{d-1} \mathrm{d}\xi$, which is large when the dimension d increases. These two different scalings actually lead to the same slope of $L(t)$ on the log scale, i.e. $(\log(L)/\log(T-t)) \approx \frac{1}{2}$, and also to the same decay property of $a(\tau)$, when we test the cases $d = 4$ and $d = 5$. Here, the term $\int_0^\infty ... \xi^{d-1} \mathrm{d}\xi$ can be reduced to the order $\int_{-1}^{1-\delta_0} ... (1-z)^{3.5-d} \mathrm{d}z$ by calculating the qunatity $a(\tau)$ from the variable z, where $\delta_0 = 1 - z_N$ and z_N is the second last discretized Chebyshev–Gauss–Lobatto collocation point, i.e.

$$\begin{aligned} a(\tau) &= -\frac{2}{p\|v_0\|_{L^2}^2} \int_0^\infty |v|^{2\sigma} \mathrm{Im}\,(\bar{v}\Delta v)\, \xi^{d-1} \mathrm{d}\xi \\ &= -\frac{2}{p\|v_0\|_{L^2}^2} \int_{-1}^{1-\delta_0} |v|^{2\sigma} \mathrm{Im}(\alpha^{\frac{d}{2}-1}(1-z)^{3.5-d}(1+z)^{d-0.5} v_{zz} \\ &\quad - \alpha^{d-2}(1-z)^{2.5-d}(1+z)^{d-0.5} v_z + \\ &\quad (d-1)\alpha^{d-2}(1+z)^{d-1.5}(1-z)^{2.5-d} v_z) \frac{1}{\sqrt{(1+z)(1-z)}} \mathrm{d}z. \end{aligned}$$

Table 1. Details about the initial data used in the dimension d, $u_0 = A_0 e^{-\frac{r^2}{d}}$, also the threshold amplitude for blow-up $\tilde{A}$, and the L^2 norms of the ground state Q, $e^{-\frac{r^2}{d}}$ and u_0.

d	$\|Q\|_2^2$	$\|e^{-\frac{r^2}{d}}\|_2^2$	$\tilde{A}$	A_0	$\|u_0\|_2^2$
4	20.7129	2	3.2181	5	50
5	112.6131	6.5683	4.1406	6	236.46
6	765.0696	27	5.3231	8	1728
7	6236.3848	133.2859	6.8403	10	13 329
8	59 304.81	768	8.7875	15	172 800
9	644 519.4793	5059.0686	11.2871	20	2.0236×10^6
10	7880 266.4892	37 500	14.4962	25	2.3437×10^7
11	107 056 593.2682	308 902.5995	18.6164	30	2.7801×10^8
12	1586 849 773.5085	2799 360	23.8089	40	4.4790×10^9

Table 2. The error $\mathcal{E}$ from (2.17) on the conserved quantity $\|v(\tau)\|_{L_\xi^\infty} \equiv 1$ in τ by using the predictor-corrector method (2.14) and (2.15) with $\delta\tau = 2 \times 10^{-3}$.

d	4	5	6	7	8	9	10	11	12
$\mathcal{E}$	6×10^{-9}	5×10^{-10}	1×10^{-9}	1×10^{-9}	1×10^{-9}	1×10^{-9}	2×10^{-9}	3×10^{-10}	9×10^{-10}

The second time step $v^{(1)}$ can be obtained by the standard second order explicit Runge–Kutta method (RK2). We stopped our simulations at the dimension $d = 12$, see details and discussion on this in section 3.

2.2. Numerical results

2.2.1. Initial data. As in [30], we use the Gaussian-type data $u_0(r) = Ae^{-r^2}$ as the initial data[2], which leads to the self-similar blow-up solutions concentrated at the origin (Towerne profiles). We actually work with data $u_0 = A_0\, e^{-\frac{r^2}{d}}$. The reason for not taking $u_0 = A\, e^{-r^2}$ as the initial data is that the amplitude A_0 becomes very large in higher dimensions; while the normalization term $\frac{r^2}{d}$ allows us to keep A_0 reasonably small. The typical initial data is given in table 1.

This table lists the mass of the ground state Q, the mass of $e^{-\frac{r^2}{d}}$, and we also list the threshold of the amplitude $\tilde{A}$ for the blow-up versus global existence. We list an example of the amplitude A_0 that we use in our simulations to be specific, though any amplitude $A_0 > \tilde{A}$ gives the same result.

Our next table 2 shows how the quantity $\|v\|_{L_\xi^\infty}$ is conserved in the rescaled time τ, i.e. we track the error

$$\mathcal{E} = \max_\tau(\|v(\tau)\|_{L_\xi^\infty}) - \min_\tau(\|v(\tau)\|_{L_\xi^\infty}). \tag{2.17}$$

We comment that one should avoid choosing initial data too flat around the origin, for example, something like super-Gaussian data $u = A_0 e^{-r^4}$, since this may lead to the collapsing rings instead of the Towerne profiles which we are trying to track here, for example, see [9, 17, 19, 20].

[2] We also ran simulations with the ground state-type of initial data $u_0 \sim Ae^{-r}$, and the results were similar. For brevity, we only include the discussion on the Gaussian-type data.

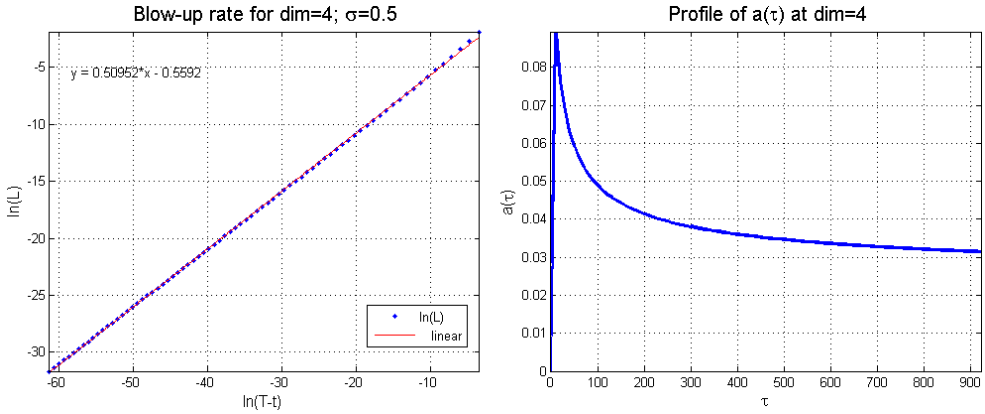

Figure 2. The 4D case: the slope of $L(t)$ on the log scale (left); the behavior of $a(\tau)$ (right).

2.2.2. Blow-up rate. We discuss our numerical results in the case $d = 4$, the results for the dimensions $d = 5, ..., 12$ are similar, we omit them here, and refer the reader to [54]. We first observe that

$$L(t) \sim \sqrt{T - t}, \tag{2.18}$$

see figures 2. The slope of $L(t)$ in the log scale is shown on the left, where we plotted $\log(T - t)$ versus $\log(L)$; it gives a straight line with the slope approximately $\frac{1}{2}$ (the slope is 0.503 01 in figure 2 (left). This confirms the square root in (2.18). We remark that for $d = 2$ and $d = 3$ similar computations and graphs were obtained in [30].

Our next task is to obtain the correction term in the rate (2.18). For that, as it is discussed in [44], one has to study the behavior of $a(\tau)$, defined in (2.2)–(2.4). We show the behavior of $a(\tau)$ in figure 2 on the right; the graph shows a very slow decay of $a(\tau)$, which is also similar to the 2D case in [30].

The formal asymptotic analysis in [24] (see also [44, section 8]) investigates the decay rate of $a(\tau)$. For that, first, substituting $v = \mathrm{e}^{\mathrm{i}\tau - ia\xi^2/4} w$ into (2.2), the equation for w is obtained:

$$iw_\tau + \Delta w - w + \frac{1}{4} b(\tau)\xi^2 w + |w|^{2\sigma} w = 0, \tag{2.19}$$

where $b(\tau) = a^2 + a_\tau = -L^3 L_{tt}$. Then, studying the asymptotic behavior of solutions to (2.19), a description of the asymptotic form of collapsing solutions very close to singularity is given in [44, section 8.2]. In particular, [44, proposition 8.5] shows the following behavior of parameters:

$$a = -L_t L, \qquad \tau_t = L^{-2}, \qquad L^3 L_{tt} = -b, \tag{2.20}$$

where

$$b = a^2 + a_\tau \approx a^2 \quad \text{obeys} \quad b_\tau = -\frac{2N_c}{M}\nu(\sqrt{b}) \approx -\frac{2\nu_0^2}{M}\mathrm{e}^{-\pi/\sqrt{b}} \tag{2.21}$$

(thus, $a_\tau \ll a^2$) with

$$N_c = \int_0^\infty Q^2 r^{d-1}\,\mathrm{d}r, \quad M = \frac{1}{4}\int r^2 Q^2 r^{d-1}\,\mathrm{d}r \quad \text{and} \quad \nu_0 = \lim_{r\to\infty} e^r r^{\frac{d-1}{2}} Q(r).$$

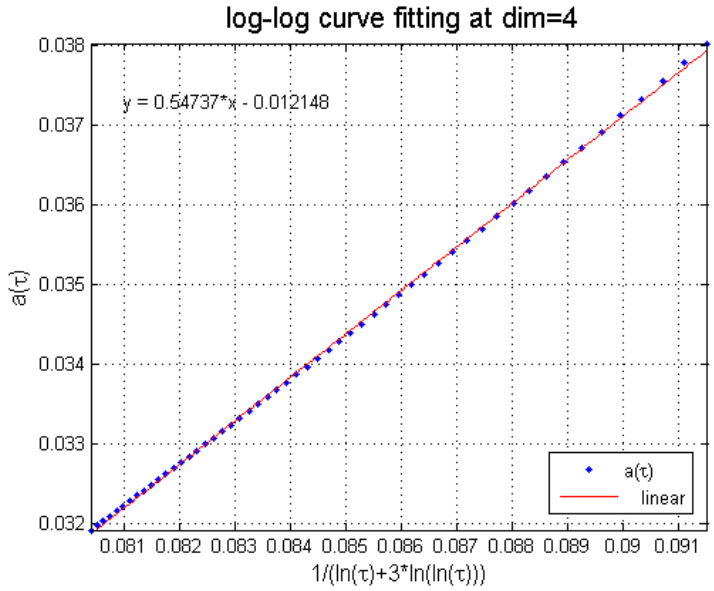

Figure 3. The curve fitting for the $a(\tau)$ for 4D case. This initially suggests that $a(\tau) \sim 1/(\ln\tau + 3\ln\ln\tau)$.

The above characterization of parameters was first derived by Fraiman in 1985 [13] via perturbation arguments for the linear stability analysis around Q, and independently by Papanicolaou *et al* in [26] and [24] via a solvability condition from considering dimension as a continuous variable decreasing down to the L^2-critical value $\frac{2}{\sigma}$. At the first leading order, as $\tau \to \infty$, it was shown that $a(\tau) \approx b^{1/2}$ decays at the following rate

$$a(\tau) \approx b^{1/2} \sim \frac{\pi}{\ln\tau},$$

i.e. slower than any polynomial rate in τ, see [44, proposition 8.6]. When more corrective terms are retained, then

$$a(\tau) \approx \frac{\pi}{\ln\tau + c\cdot\ln\ln\tau},$$

and from $a_\tau \approx -\frac{\nu_0^2}{M}a^{-1}\mathrm{e}^{-\pi/a}$ (consequence of the solvability condition) one concludes that $c = 3$. Furthermore, the scaling factor $L(t)$ has the asymptotic form

$$L(t) \approx \left(\frac{2\pi(T-t)}{\ln\ln(\frac{1}{T-t})}\right)^{\frac{1}{2}}. \tag{2.22}$$

Following [24], we further investigate numerically the correction term in $L(t)$ in (2.18) and study the slope of $a(\tau)$ as a function of $1/(\ln\tau + 3\ln\ln\tau)$. In figure 3, we observe that the function $a(\tau)$ versus $1/(\ln\tau + 3\ln\ln\tau)$ is a straight line. It would now be very tempting to make a conclusion that $a(\tau) \sim 1/(\ln\tau + 3\ln\ln\tau)$, as it was also predicted in $d = 2$ in [24] and [26]. However, more care is needed here.

If we change the constant c dependence in the second term of $1/(\ln\tau + c\ \ln\ln\tau)$ and try to investigate the slope of $a(\tau)$ as a function of $1/(\ln\tau + c\ln\ln\tau)$ for different c, including zero and large constants (we tried $c = 0, 1, 3, 100, 1000$), we find that the slope does not change,

which only confirms that such a correction is difficult to investigate numerically, since it only happens at the very high focusing levels. Also, one notes that the slope of the line is not $\frac{1}{\sqrt{2\pi}}$ as expected from asymptotic analysis from [24], where it states that the correction term for $a(\tau)$ is given by

$$q(t) \approx \left(\frac{2\pi}{\ln \ln \frac{1}{|T-t|}} \right)^{\frac{1}{2}}.$$

This is because at the time we stop our simulations (we are forced to stop as the maximal machine's precision is reached), the values of $a(\tau)$ are still far from zero, this is also observed in [24, 26, 44]. Hence, further justification for the correction term is needed and we discuss it in the next subsection.

2.2.3. Further justification of 'log–log' correction. In [9, chapter 18], Fibich shows that the log–log regime is reached when the focusing amplitude of the solution is extremely large (e.g. a necessary condition for the log–log to hold in dimension 2 is $A \gg 10^{48}$), which is basically impossible to observe numerically (although see [27] for even higher order correction terms in the blow-up rate). Instead he suggests studying the reduced equations, where the equations (2.20) and (2.21) are written in the following form

$$b_\tau(\tau) = -\nu(b), \qquad a_\tau(\tau) = b - a^2, \tag{2.23}$$

where $\nu(b) = c_\nu \, \mathrm{e}^{-\pi/\sqrt{b}}$ with $c_\nu = 2\nu_0^2/M$. Our numerical calculations give $c_\nu \approx 44.8$ in $d = 2$ (matching section 17.7 in [9]) and $c_\nu \approx 53.11$ in $d = 4$. The advantage of working with the system (2.23) as mentioned in [9] is that it can be solved by standard numerical methods over hundreds of orders of magnitudes without a significant deterioration in the numerical accuracy. We solve this system by RK2 and then recover $L(\tau)$ and $T - t$ from numerical quadratures of

$$L(\tau) = L(0)\mathrm{e}^{-\int_0^\tau a(s)\mathrm{d}s}, \qquad T - t = \int_\tau^\infty \frac{\mathrm{d}t}{\mathrm{d}\tau}\mathrm{d}\tau = \int_\tau^\infty L^2(\tau)\mathrm{d}\tau. \tag{2.24}$$

We show our results for $d = 4$ in figure 4. On the left subfigure in figure 4, we plot the behavior of $b(t)$ as a function of $L(t)$ for three approximations: a solid blue line is the numerical solution, a dash–dot pink (straight) line is a strict adiabatic approximation $b(t) \equiv b(0) = 10^{-1}$ and the dashed green line is an asymptotic approximation of the log–log law $b(\tau) \sim \frac{\pi^2}{\ln^2 \tau}$. One can see that even when the amplitude reaches focusing of 10^{250} (i.e. $L(t) \sim 10^{-250}$) the log–log law is further away from the numerical solution than the strict adiabatic law, though it is slowly decreasing down.

On the right subfigure in figure 4 the ratio $L(t)/L_{\log\log}$ is shown, where $L_{\log\log} = \left(\frac{2\pi(T-t)}{\ln\ln(\frac{1}{T-t})}\right)^{\frac{1}{2}}$ is the anticipated blow-up rate. It is slowly growing towards one, however, still a bit far from it. These figures also show that there is an intermediate adiabatic regime in the blow-up dynamics, which asymptotically approaches the log–log regime. The adiabatic laws are obtained in [12] and [28], and further discussed in [9].

While it is challenging to observe the log–log correction term numerically, in [1] the functional form testing was suggested and the authors succeeded in showing that among all tested functional forms, the log–log form stabilized the power 1/2 in the rate approximation (2.25) and also minimized the fitting errors the best as the computation increased focusing levels.

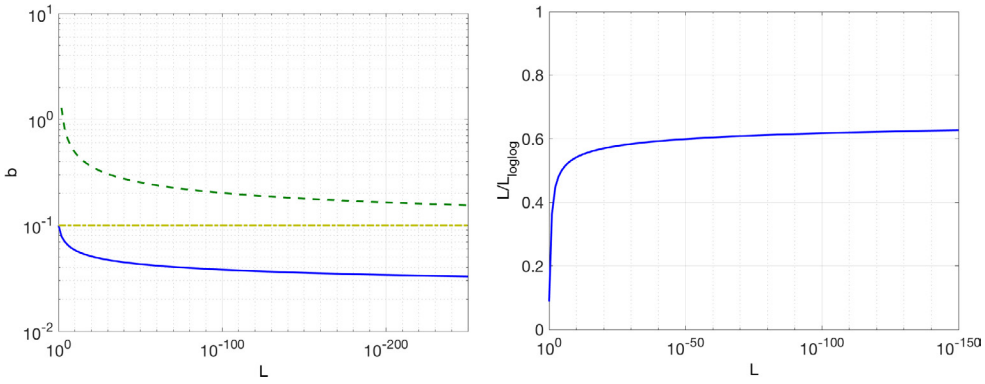

Figure 4. The reduced equations (2.23) and (2.24) in $d = 4$, $b(0) = 0.1$, $L(0) = 1$, and $L_t(0) = 0$. Left: $b(t)$ as a function of $L(t)$, where solid curve is a numerical solution of the reduced system (2.23), dashdot curve is a strict adiabaticity $b \equiv b(0)$, and dash curve is an asymptotic approximation for the log–log law. Right: the ratio of $L(t)/L_{\log\log}$.

Moreover, the authors were able to show that before the log–log regime, the blow-up mechanism seemed to follow the adiabatic regime. Specifically, it was supposed in [1] that

$$\frac{1}{L(t)} \sim \left(\frac{F(T-t)}{T-t}\right)^{\frac{1}{2}}, \tag{2.25}$$

where $F(s) = \left(\ln \frac{1}{s}\right)^{\gamma}$, $\gamma = 1, 0.6, 0.5, 0.4, ..., 0$, or $F(s) = \ln\ln \frac{1}{s}$. Then $\frac{1}{L(t_i)}$ was computed at the time t_i as well as the approximation parameter

$$\rho_i = \frac{L(t_i)}{L(t_{i+1})} \Big/ \ln\left(\frac{F_{i+1}/(T-t_{i+1})}{F_i/(T-t_i)}\right). \tag{2.26}$$

Since the power ρ is expected to be $\frac{1}{2}$ (after all it is square root decay), one can check how fast the parameter ρ_i converges to $\frac{1}{2}$ and what choice of $F(s)$ gives the best approximation. In [1] it was shown that $F(s) = \ln\ln \frac{1}{s}$ provides the fastest and best parameter ρ_i *stabilization*, moreover, it also gives the optimal quantity in several error estimates such as the standard deviation, l^1-norm discrepancy, and l^2-norm discrepancy, which gave an extra assurance of $\ln\ln \frac{1}{s}$ selection for $F(s)$.

In our further numerical investigation of the correction term, we use this functional approach as well. We observe that the 'log–log' correction does stabilize the power ρ close to $\frac{1}{2}$ the best, and it minimizes the approximation errors quite good (eventually) in the functional fitting. For this purpose, we compute $\frac{1}{L(t)}$ as defined in (2.25), ρ_i as defined in (2.26), and ϵ_i, the l^2 discrepancy, defined as (following [1])

$$\epsilon_i = \left[\frac{1}{i - j_0 + 1}\sum_{j=j_0}^{i}\left(\frac{1}{2} - \rho_j\right)^2\right]^{\frac{1}{2}}. \tag{2.27}$$

Before proceeding with our fitting results, one other remark is needed. We need to specify the process of calculating the quantity $(T - t_i)$. We take the blow-up time T to be the time when we end our simulation. We have $L(\tau_{i+1}) = \exp(\ln L(\tau_{i+1}))$. Denoting $\Delta t_{i+1} := t_{i+1} - t_i$, and from the last equation of (2.1),

Table 3. Comparison of the different functional forms $F(s)$ for the correction term in $d = 4$. '$\frac{1}{L(t)}$ range' means the values $\frac{1}{L(t_i)} \sim \frac{1}{L(t_{i+1})}$. The blow-up rate ρ seems to fit close to 0.5 in the intermediate regime for $F(s) = (\ln \frac{1}{s})^{\gamma}$ (for example, for $i = 3, 4$ with $\gamma = 0.25$; for $i = 7, 8, 9$ with $\gamma = 0.2$), however, the best stabilization of the power is given by the log–log correction.

The fitting power ρ_i from different corrections for $F(s)$							
i	$\frac{1}{L(t)}$ range	1	$(\ln \frac{1}{s})^{0.3}$	$(\ln \frac{1}{s})^{0.25}$	$(\ln \frac{1}{s})^{0.2}$	$(\ln \frac{1}{s})^{0.15}$	$\ln \ln \frac{1}{s}$
0	$1 \times 10^4 \sim 3 \times 10^5$	0.5084	0.5006	0.5019	0.5032	0.5045	0.4997
1	$3 \times 10^5 \sim 7 \times 10^6$	0.5056	0.5003	0.5008	0.5018	0.5027	0.4997
2	$7 \times 10^6 \sim 1 \times 10^8$	0.5042	0.4998	0.5003	0.5011	0.5019	0.4997
3	$1 \times 10^8 \sim 2 \times 10^9$	0.5033	0.4995	0.5000	0.5007	0.5013	0.4997
4	$2 \times 10^9 \sim 4 \times 10^{10}$	0.5028	0.4994	0.4999	0.5004	0.5010	0.4997
5	$4 \times 10^{10} \sim 6 \times 10^{11}$	0.5023	0.4994	0.4998	0.5003	0.5008	0.4997
6	$6 \times 10^{11} \sim 8 \times 10^{12}$	0.5020	0.4993	0.4997	0.5002	0.5006	0.4997
7	$8 \times 10^{12} \sim 1 \times 10^{14}$	0.5018	0.4993	0.4997	0.5001	0.5005	0.4997
8	$1 \times 10^{14} \sim 1 \times 10^{15}$	0.5016	0.4993	0.4997	0.5000	0.5004	0.4997
9	$1 \times 10^{15} \sim 2 \times 10^{16}$	0.5014	0.4993	0.4996	0.5000	0.5004	0.4997

$$\Delta t_{i+1} = \delta\tau L^2(\tau_{i+1}). \tag{2.28}$$

Thus, the mapping for rescaled time τ back to the real time t is calculated as

$$t(\tau_{i+1}) = t((i+1)\delta\tau) := \sum_{j=1}^{i+1} \Delta t_j = \delta\tau \sum_{j=0}^{i+1} L(\tau_j)^2. \tag{2.29}$$

Note that as time evolves, the time difference $T - t(\tau_i)$ will become smaller and smaller, and eventually reach saturation level (with little change), therefore we treat the stopping time $t(\tau_{\text{end}}) = t(\tau_M)$ as the blow-up time T where M is the total number of iterations when reaching the stopping condition ($L < 10^{-17}$). Then, we can take

$$T = t(\tau_{\text{end}}) = t(M\delta\tau) = \delta\tau \sum_{j=0}^{M} L(\tau_j)^2. \tag{2.30}$$

Consequently for any t_i, we can calculate $T - t_i$ as

$$T - t_i = \sum_{j=i+1}^{M} \Delta t_j = \delta\tau \sum_{j=i+1}^{M} L(\tau_j)^2. \tag{2.31}$$

This indicates that instead of recording the cumulative time t_i, we just need to record the elapsed time between the two recorded data points, i.e. $\Delta t_i = t_{i+1} - t_i$. By doing so, it can avoid the loss of significance when adding a small number onto a larger one.

Continuing with the functional fitting for the correction term, we tried several choices for $F(s)$, namely, $F(s) = 1$, $F(s) = \left(\ln \frac{1}{s}\right)^{\gamma}$, $\gamma = 0.5, 0.4, 0.3, 0.25, 0.2, 0.15, 0.1$ and $F(s) = \ln \ln \frac{1}{s}$.

In the dimension $d = 4$, while studying the parameter ρ_i, we observe that out of all different powers of γ that we tried, mentioned above, in the fitting of $F(s) = \left(\ln \frac{1}{s}\right)^{\gamma}$, the powers 0.25 and 0.2 seem to approximate the rate $\frac{1}{2}$ the best, see table 3 for values of ρ_i. In

Table 4. Comparison of the l^2 discrepancy ϵ_i in the fitting of different correction terms in $d = 4$. One can see that the log–log correction minimizes this error the best.

The l^2 discrepancy ϵ from different corrections $F(s)$							
i	$\frac{1}{L(t)}$ range	1	$(\ln\frac{1}{s})^{0.3}$	$(\ln\frac{1}{s})^{0.25}$	$(\ln\frac{1}{s})^{0.2}$	$(\ln\frac{1}{s})^{0.15}$	$\ln\ln\frac{1}{s}$
0	$1\times10^4\sim3\times10^5$	0.0084	6.45×10^{-4}	0.0019	0.0032	0.0045	3.34×10^{-4}
1	$3\times10^5\sim7\times10^6$	0.0072	4.70×10^{-4}	0.0015	0.0026	0.0037	3.21×10^{-4}
2	$7\times10^6\sim1\times10^8$	0.0063	4.75×10^{-4}	0.0012	0.0022	0.0032	3.18×10^{-4}
3	$1\times10^8\sim2\times10^9$	0.0057	5.19×10^{-4}	0.0011	0.0019	0.0029	3.17×10^{-4}
4	$2\times10^9\sim4\times10^{10}$	0.0053	5.60×10^{-4}	9.42×10^{-4}	0.0017	0.0026	3.14×10^{-4}
5	$4\times10^{10}\sim6\times10^{11}$	0.0049	5.92×10^{-4}	8.65×10^{-4}	0.0016	0.0024	3.11×10^{-4}
6	$6\times10^{11}\sim8\times10^{12}$	0.0046	6.15×10^{-4}	8.07×10^{-4}	0.0015	0.0022	3.08×10^{-4}
7	$8\times10^{12}\sim1\times10^{14}$	0.0044	6.31×10^{-4}	7.63×10^{-4}	0.0014	0.0021	3.04×10^{-4}
8	$1\times10^{14}\sim1\times10^{15}$	0.0041	6.54×10^{-4}	7.29×10^{-4}	0.0013	0.0020	2.99×10^{-4}
9	$1\times10^{15}\sim2\times10^{16}$	0.0040	6.50×10^{-4}	7.00×10^{-4}	0.0012	0.0019	2.95×10^{-4}

Table 5. Comparison of the l^2 discrepancy ϵ_i computed in the window from $j_0 = 7$ to $i = 9$ in the fitting of different correction terms in $d = 4$.

$F(s)$	1	$(\ln\frac{1}{s})^{0.3}$	$(\ln\frac{1}{s})^{0.25}$	$(\ln\frac{1}{s})^{0.2}$	$(\ln\frac{1}{s})^{0.15}$	$\ln\ln\frac{1}{s}$
ϵ	0.0017	7.28×10^{-4}	3.24×10^{-4}	1.06×10^{-4}	5.00×10^{-4}	2.69×10^{-4}

fact, one can first observe that the functional forms $\left(\ln\frac{1}{s}\right)^{\gamma}$ decrease down to the power $\frac{1}{2}$ quite well, for example, $\gamma = 0.25$ gives the best approximation on steps $i = 3, 4, 5$ (or corresponding time intervals) as it is the closest to $\frac{1}{2}$; $\gamma = 0.2$ gives the best approximation on steps $i = 6, 7, 8, 9$. However, the second observation is that all such forms tend to decrease down to the power $\frac{1}{2}$ and then continue decreasing further down (for example, the form with $\gamma = 0.25$ starts decreasing on steps $i = 4, 5, ..., 9$ but then underperforms at the step $i = 9$ compared to the log–log form), thus, eventually not representing the appropriate correction. Note that the functional form, which stabilizes well and stays quite close to $\frac{1}{2}$, is the log–log form.

The first observation is due to the existence of an intermediate regime in the blow-up dynamics, the adiabatic regime. The second observation is indicating that the adiabatic regime goes asymptotically into the log–log regime.

We also computed the l^2 discrepancy ϵ_i, defined by (2.27), starting from the step $j_0 = 0$ and accumulating up to the step i, and show the results in table 4. We note that in the dimension $d = 4$ this cumulative error is minimized the best by the log–log correction. Since the log–log regime is an asymptotic regime, we also computed the l^2 discrepancy error starting from $j_0 = 7$ and up to the last reliable step $i = 9$, i.e. for the window of the three last approximations (see also the discussion about the window of approximations in [1]), and recorded it in table 5. While one can observe that the form $F(s) = \left(\ln\frac{1}{s}\right)^{0.2}$ minimizes the discrepancy ϵ_i the best in table 5, it is because this specific power of $\gamma = 0.2$ decreases down to $\frac{1}{2}$ the closest at that specific window. However, as discussed above, we expect it to keep decreasing, and thus, getting further away from $\frac{1}{2}$. In general, we suspect that all functional forms $\left(\ln\frac{1}{s}\right)^{\gamma}$ will for some period of time approximate the power $\frac{1}{2}$ well, but then will escape away from $\frac{1}{2}$, and thus, destabilize away from the blow-up regime. This is, of course, an area for further challenging numerical investigations, as well as possible testing of adiabatic regimes given by Malkin

Table 6. Comparison of the different functional forms $F(s)$ for the correction terms in $d = 5$. '$\frac{1}{L(t)}$ range' means the values $\frac{1}{L(t_i)} \sim \frac{1}{L(t_{i+1})}$. While all other forms give a slow decrease, the loglog form seems to stabilize to the power 1/2 the best.

The fitting power ρ_i from different corrections for $F(s)$							
i	$\frac{1}{L(t)}$ range	1	$(\ln\frac{1}{s})^{0.3}$	$(\ln\frac{1}{s})^{0.25}$	$(\ln\frac{1}{s})^{0.2}$	$(\ln\frac{1}{s})^{0.15}$	$\ln\ln\frac{1}{s}$
0	$2\times10^3 \sim 6\times10^4$	0.5093	0.4998	0.5013	0.5029	0.5045	0.4977
1	$6\times10^4 \sim 2\times10^6$	0.5060	0.4994	0.5005	0.5015	0.5026	0.4989
2	$2\times10^6 \sim 4\times10^7$	0.5044	0.4992	0.5001	0.5009	0.5018	0.4993
3	$4\times10^7 \sim 7\times10^8$	0.5034	0.4991	0.4999	0.5006	0.5013	0.4994
4	$7\times10^8 \sim 1\times10^{10}$	0.5028	0.4991	0.4997	0.5004	0.5010	0.4995
5	$1\times10^{10} \sim 2\times10^{11}$	0.5024	0.4991	0.4997	0.5002	0.5007	0.4996
6	$2\times10^{11} \sim 3\times10^{12}$	0.5020	0.4992	0.4996	0.5001	0.5006	0.4996
7	$3\times10^{12} \sim 5\times10^{13}$	0.5018	0.4992	0.4996	0.5001	0.5005	0.4996
8	$5\times10^{13} \sim 7\times10^{14}$	0.5016	0.4992	0.4996	0.5000	0.5004	0.4997
9	$7\times10^{14} \sim 1\times10^{16}$	0.5014	0.4992	0.4996	0.5000	0.5003	0.4997

Table 7. The l^2 discrepancy ϵ starting from $j_0 = 7$ to $i = 9$ in the fitting of different correction terms in $d = 5$. This means we only consider the behaviors close to blow-up. One can see the log–log correction minimizes the deviation the best at this stage.

$F(s)$	1	$(\ln\frac{1}{s})^{0.3}$	$(\ln\frac{1}{s})^{0.25}$	$(\ln\frac{1}{s})^{0.2}$	$(\ln\frac{1}{s})^{0.15}$	$\ln\ln\frac{1}{s}$
ϵ	0.0017	7.98×10^{-4}	3.81×10^{-4}	6.74×10^{-4}	4.65×10^{-4}	3.41×10^{-4}

adiabatic law [28] and Fibich adiabatic law [9]. We note that the second best approximation in table 5 is produced by the log–log form.

For dimension five we do a similar investigation and list the results of the functional fittings for $F(s) = 1, \left(\ln\frac{1}{s}\right)^{0.3}, \left(\ln\frac{1}{s}\right)^{0.25}, \left(\ln\frac{1}{s}\right)^{0.2}, \left(\ln\frac{1}{s}\right)^{0.15}$, and $\ln\ln\frac{1}{s}$, in table 6. One can observe that the forms of type $\left(\ln\frac{1}{s}\right)^{\gamma}$ give decreasing ρ_i as the step i increases; some of them reach the value 0.5 during the calculated time period ($\gamma = 0.25, 0.2$) and some might reach it eventually ($\gamma = 0.15$). However, the continuing decrease of ρ_i values does not perform as good as the stabilization seen in the log–log form.

We supply the l^2 discrepancy errors ϵ_i for the window $j_0 = 7$ to $i = 9$ (the last 3 steps) in table 7, where the loglog fit has the smallest l^2 deviation.

We provide computations for the functional fittings for other dimensions in appendix A.

Putting all our numerical calculations, asymptotical analysis and functional fitting results together, we conclude that the blow-up rate $L(t)$ (with the first term correction) is given by (2.22).

2.2.4. Blow-up profile. In this subsection we investigate profiles of the blow-up solutions, and show our results in dimensions $d = 4$. Figure 5 shows how the blow-up solutions $v = v(\xi, \tau)$ from (2.2) converge to the rescaled ground state Q, which leads to the conclusion that the profile is given by the rescaled (self-similar) version of the corresponding ground state $\frac{1}{L^{1/\sigma}}Q(\frac{r}{L})$.

We plot three different times snapshots ($\tau = 2, 40, 400$) and list the time values in both τ and t variable (it is easier to distinguish and track the profiles in the rescaled τ variable, as $\tau \to \infty$, than in the variable t, which converges to some finite time $0 < T < \infty$, and thus, t maybe indistinguishable very close to T). The results for other dimensions are similar, see in [54].

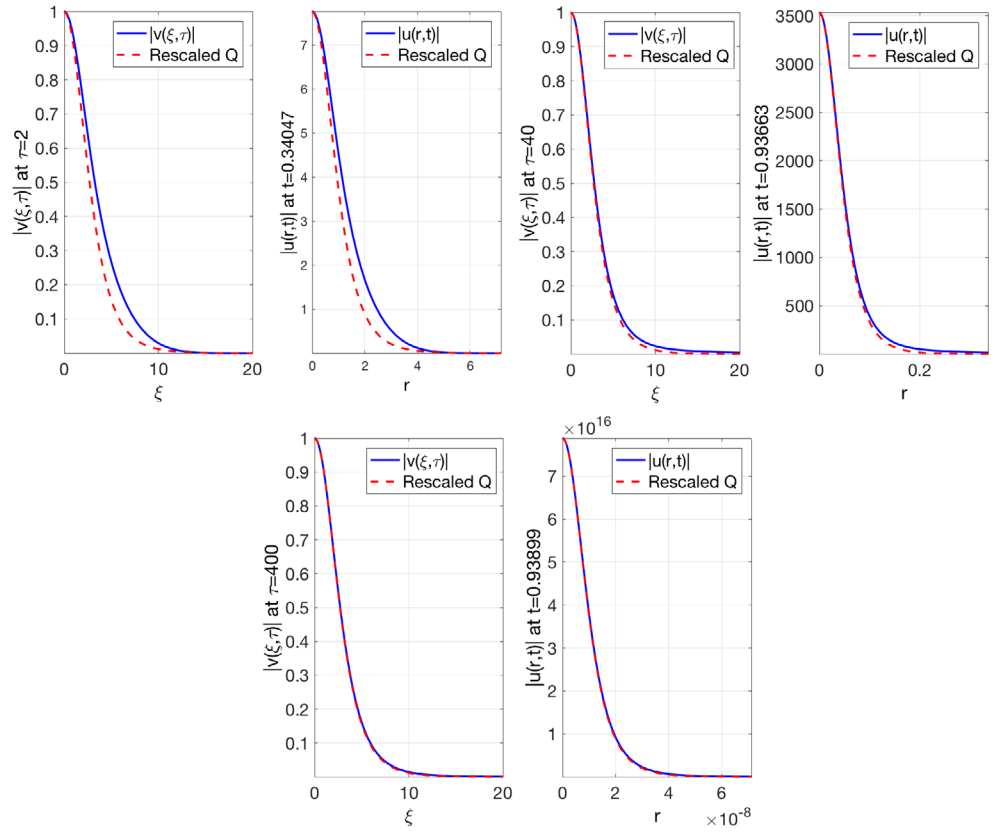

Figure 5. Blow-up profile for $d = 4$. The blow-up solution converges to the ground state Q. Here, the 'Rescaled Q' means $\frac{1}{L^{1/\sigma}} Q\left(\frac{r}{L}\right)$.

To summarize, our numerical simulations confirm that a generic blow-up in higher dimensions (in the L^2-critical NLS) has the log–log regime characteristics (rate and profile), and our next goal is to justify these observations rigorously.

The analytical proof of the log–log blow-up regime (including higher dimensions) was given in several works of Merle and Raphaël, [33–35], provided the spectral property 1 holds. In [10], the authors were able to check it in dimensions $d = 2, 3, 4$ (up to some corrections in [11]) and in the next section we investigate higher dimensions $d \geqslant 5$, while confirming the results for the low dimensions in appendix D.

3. Spectral properties

The stable 'log–log' blow-up regime for the initial data with the mass slightly above the ground state mass, $M[Q]$, negative energy and zero momentum[3] for the 1D case was proved by Merle and Raphaël in [33] and [34], see also the work of Galina Perelman [37] in 1D. In [33] and [34] a proof of theorem 1.3 in higher dimensions was also given, assuming the spectral property 1 holds true. A major obstacle for obtaining spectral properties in higher dimensions is the lack of explicit expression for the ground state Q. In 2006, Fibich, Merle and Raphaël

[3] Or the energy is adjusted for the non-zero momentum.

made an attempt to check that the spectral property 1 holds true with a numerically-assisted proof for the dimensions up to $d = 5$ in [10].

Before we proceed to study the spectral property 1 in higher dimensions ($d \geqslant 5$), we want to check if the methods from [10] would allow higher dimensional generalization and verification. We first address the choice of the boundary conditions in [10] (see also [29]). The solution $u(x,t)$ lives in the following space:

$$\left\{ u \text{ is radial} : \int |\nabla u|^2 + |u|^2 \mathrm{e}^{-\gamma_0 |x|} < \infty \right\}.$$

This implies that $u_r(r) \to 0$ as $r \to \infty$, or equivalently, $u(r) \to C$ as $r \to \infty$. On the other hand, from the analysis of the operators L_1 and L_2, we know that $(1 + r^{d-2})u \in L^\infty(\mathbb{R}^d)$. In $d = 2$, this means that $u \in L^\infty(\mathbb{R}^2)$, or in other words, $u(r) \to C$ as $r \to \infty$ with C not necessarily being zero. For $d \geqslant 3$, the last condition implies $|u(r)| < \frac{C}{1+r^{d-2}}$, and hence, $u(\infty) = 0$. Thus, using the boundary conditions $u_r(L) = 0$ in $d = 3, 4, 5$ in [10] makes the results less reliable, though the outcome is not affected in $d = 3, 4$. For clarification, we include table 12 as the comparison between the application of the two different boundary conditions in dimension $d = 5$. We also included a comparison for dimensions $d = 2, 3, 4$ in appendix D.

As far as the higher dimensions $d \geqslant 6$, we think that one of the reasons that the methods from [10] can not handle $d \geqslant 6$ is also the use of the boundary conditions $u_r(L) = 0$ for sufficiently large L (say $L = 20$ or $L = 30$), instead of $u(\infty) = 0$. In this paper, we use the boundary condition $u(\infty) = 0$. We also note that the same approach was used in [29] for analyzing the 3D cubic NLS equation. Our simulations show that the spectral properties holds for $d \leqslant 10$ for general case (not necessarily radial), and also for $d = 11$ and $d = 12$ in the radial case. We stopped our calculations at $d = 12$, since the magnitude as well as the L^2 norm of the ground state became too large, and, computationally, it was not reliable to guarantee the accuracy. Moreover, the index of both operators L_1 and L_2 becomes increasingly more challenging to obtain numerically as the dimension d increases beyond 12.

3.1. The radial case

In this section, we show that the spectral property 1 holds true from $d = 5$ to $d = 12$, and the spectral property 2 holds for $d = 2...12$. We first recall the definitions of an index of a bilinear form B, see, for example, [10] and [29]:

Definition 3.1 (Index of a bilinear form). The index of a bilinear form B with respect to a vector space $\mathbf{V}$ is

$$\mathrm{ind}_V(B) = \min\{k \in \mathbb{N} \,|\, \text{there exists a sub-space } P \text{ of codimension } k \text{ such that } B_{|P} \text{ is positive}\}.$$

Let B_1 and B_2 be the bilinear forms associated with the operators L_1 and L_2, see (1.10) and (1.11) in definition (1.1). Note that the $\mathrm{ind}_{H^1}(B_{1,2})$ equals to the number of negative eigenvalues of $L_{1,2}$. Therefore, we often refer to $\mathrm{ind}(L_{1,2})$ as the number of negative eigenvalues of $L_{1,2}$.

Since the potential term $V_{1,2}$ is smooth and decays exponentially fast, according to theorem XIII.8 in [40], which is a generalization of the Sturm oscillation theorem (section XIII.7 of [40]), the operators $L_{1,2}$ have finite number of negative eigenvalues. Moreover, the number of the negative eigenvalues can be estimated by counting the number of zeros of the solutions to the following ODE:

Table 8. Values of the quantities from proposition 3.1 at $r_0 = 6$.

d	5	6	7	8
$\partial_r u(r_0)u(r_0)$	1.4009×10^{-05}	4.7096×10^{-05}	1.9375×10^{-05}	6.2832×10^{-06}
$-V_1(r_0) - \frac{d-2}{4r_0}$	$-0.311\,66$	$-0.539\,61$	$-0.825\,91$	-1.1703
d	9	10	11	12
$\partial_r u(r_0)u(r0)$	1.8316×10^{-06}	4.802×10^{-07}	1.0135×10^{-07}	6.9127×10^{-09}
$-V_1(r_0) - \frac{d-2}{4r_0}$	-1.5731	-2.0343	-2.5543	-3.1335

$$\begin{cases} -\partial_{rr}U - \frac{d-1}{r}\partial_r U + V_{1,2}(r)U = 0, \\ U(0) = 1, \quad U_r(0) = 0. \end{cases} \tag{3.1}$$

The ODE (3.1) is a standard IVP problem, which can be solved, for example, by matlab solver '`ode45`'. Note that when $r \gg 1$, the equation (3.1) is essentially free (i.e. the potential term can be neglected), see [29], and consequently, the solution must behave as

$$U(r) \approx C_1 + \frac{C_2}{r^{d-2}}. \tag{3.2}$$

For the L_1 case, we apply the following statement, which is from [11]. According to this proposition, the numerical values in table 8 suggest that there will be no more intersections for $r_0 \geqslant 6$.

Proposition 3.1 (Criterion for the positivity of u, [11]). *Let u be a radial solution to*

$$-u_{rr}(r) - \frac{d-1}{r}u_r - Vu = 0, \quad \text{on } r > 0.$$

Let $V_+ = max\{V, 0\}$. Assume that there holds for some $r_0 > 1$

$$\partial_r u(r_0)u(r_0) > 0$$

and

- for $d \geqslant 3$,

$$\forall r \geqslant r_0, \quad V_+(r) \leqslant \frac{(d-2)^2}{4r^2};$$

- *for $d = 2$,*

$$\forall r \geqslant r_0, \quad V_+(r) \leqslant \frac{1}{4r^2(\log r)^2}$$

and

$$\frac{u'(r_0)}{u(r_0)} \geqslant \frac{2}{r_0}\int_{r_0}^{\infty} V_+(r)rdr.$$

Then u cannot vanish for $r \geqslant r_0$ (see table 8).

For the case of L_2, the theorem is not applicable. We adopt the argument from [29]: we first notice that the equation (3.1) converges to the free equation (3.2). Then, we choose a large

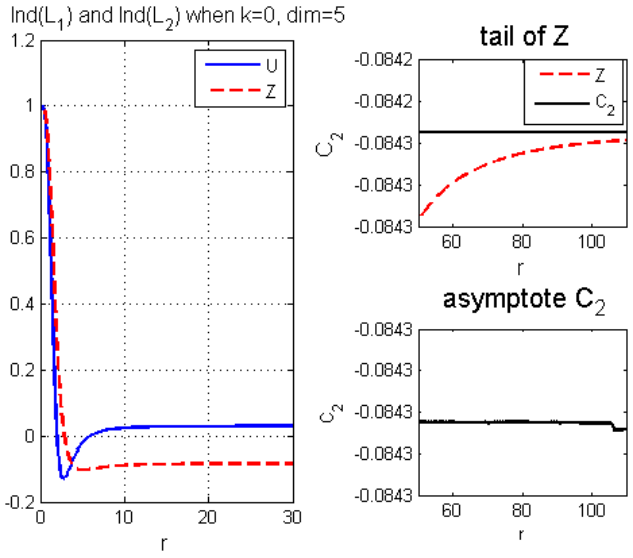

Figure 6. Solutions of (3.1) in $d = 5$. Numerical justification of proposition 3.2. The blue line shows the behavior of U from $L_1U = 0$ and the green line shows the behavior of Z from $L_2Z = 0$. We also show the behavior of the tail of Z, and the constant C_2 it approaches to as $r \to \infty$, see (3.3).

enough interval (say $L = 100$) to ensure that the solution goes to a constant. The constant can be found from

$$\begin{cases} \frac{C_1}{r_i^{d-2}} + C_2 = U_i, \\ \frac{C_1}{r_{i-1}^{d-2}} + C_2 = U_{i-1}, \end{cases} \tag{3.3}$$

where r_i and U_i are discretized points of r and $U(r)$. Once the constant C_2 starts to stabilize, we conclude that the solution enters the free region and no more 'zeros' will occur.

We also point out that one needs to be careful in the numerical calculation of the potential V_1 or V_2, since when $d \geqslant 5$, the term

$$V_2 = \frac{2}{d} Q^{\frac{4}{d}-1} r Q_r$$

generates the negative power of Q. This may fail to describe the exponential decay property, especially, when $d \geqslant 8$. An alternative way is needed to calculate the potential V_1 and V_2. We provide a new approach for that and discuss the details in the appendix C.

Our numerical solutions of the equation (3.1) are given in figure 6 as an example for the case $d = 5$, there U stands for the solution to L_1 and Z for L_2. Solutions to other dimensions of the equation (3.1) are similar. We conclude the following statement.

Proposition 3.2 (Indices of $B_{1,2}$). *For $d = 5$ to $d = 12$, the indices of $L_{1,2}$ in the radial case are*

$$\mathrm{ind}(L_1) = 2, \quad \mathrm{ind}(L_2) = 1.$$

Therefore,

$$\mathrm{ind}_{H_r^1}(B_1) = 2, \quad \mathrm{ind}_{H_r^1}(B_2) = 1.$$

The following property shows that the indices of the bilinear forms are stable under the perturbations. Thus, it is sufficient to check the terms $B_{1,2}(u,u) > 0$ instead of $B_{1,2}(u,u) > \delta_0 \int |u|^2 \mathrm{e}^{-|\mathbf{x}|}$ for some sufficiently small δ_0, given in definition 1.

Proposition 3.3 ([10, 29]). *For the operators $L_{1,2}$ (from the spectral property), there exists a universal constant $\delta_0 > 0$, sufficiently small, such that for the perturbed operators*

$$\bar{L}_{1,2} = L_{1,2} - \delta_0 \, \mathrm{e}^{-|x|},$$

the associated bilinear forms are stable, i.e.

$$\mathrm{ind}_{H^1}(\bar{B}_{1,2}) = \mathrm{ind}_{H^1}(B_{1,2}).$$

We return to the discussion of the proof of the spectral property, which involves solving the BVP problem $L_{1,2}U = f$. While the numerical calculations suggest that $L_{1,2}$ are invertible, the proof of the invertibility of the operators $L_{1,2}$ in [10] and [29] works in straightforward adaptation to our cases.

Proposition 3.4 (Invertibility of $L_{1,2}$). *Let $d \in \{5, 6, \cdots, 12\}$ and $f \in C^0_{loc}(\mathbb{R}^d)$ be radially symmetric with $|f(r)| \leqslant \mathrm{e}^{-Cr}$. Then there exists a unique radial solution to*

$$L_{1,2}u = f \quad \textit{with } (1 + r^{d-2})u \in L^\infty.$$

The following definition lists the numerical values of the bilinear forms which we need in the proof of the spectral property. It involves the computation of the BVP problem $L_{1,2}U = f$. We take $u_r(0) = 0$ as the left boundary condition, since $u(r)$ is radially symmetric. We construct the artificial boundary condition $u(L) + \frac{L}{d-2} u_r(L) = 0$ to approximate the boundary condition $u(\infty) = 0$ (see details in appendix B, also the reader can refer to [29]).

Definition 3.2 (Numerical representation of the bilinear form). Let the operator $L_i u = f$, $i = 1, 2$ solve the linear BVP

$$\begin{cases} L_{1,2}u = f, & i = 1, 2 \\ u_r(0) = 0, \quad u(\infty) = 0. \end{cases} \tag{3.4}$$

Define

$$L_1 U_1 = Q, \quad L_1 U_2 = Q_1; \tag{3.5}$$

$$L_2 Z_1 = Q_1, \quad L_1 Z_2 = Q_2; \tag{3.6}$$

and denote the following constants as values of the bilinear forms

$$K_{11} = B_1(U_1, U_1), \quad K_{22} = B_1(U_2, U_2), \quad K_{12} = B_1(U_1, U_2), \quad K_{21} = B_1(U_2, U_1); \tag{3.7}$$

$$J_{11} = B_2(Z_1, Z_1), \quad J_{22} = B_2(Z_2, Z_2), \quad J_{12} = B_2(Z_1, Z_2), \quad J_{21} = B_2(Z_2, Z_1). \tag{3.8}$$

We also define the determinants of matrices K and J by

$$KK = K_{11}K_{22} - K_{12}K_{21} \quad \text{and} \quad JJ = J_{11}J_{22} - J_{12}J_{21}. \tag{3.9}$$

We list the values of K_{ij} and J_{ij} from definition 3.2 for dimensions $5 \leqslant d \leqslant 12$ in tables 9 and 10, respectively.

Table 9. Values of the bilinear form B_1 from (3.7) and (3.9) via K_i's.

d	K_{11}	K_{12}	K_{22}	KK	$\lvert\frac{K_{12}}{K_{21}}-1\rvert$
5	−42.3114	4.515	−490.2964	20 724.7444	5×10^{-10}
6	−279.0336	23.4744	−2400.2078	669 187.6405	4×10^{-12}
7	−2199.9811	294.6847	−15 415.6211	33 827 236.411	8×10^{-11}
8	−20 133.2095	4529.9623	−119 781.6837	2391 069 177	4×10^{-11}
9	−209 271.9449	73 555.7296	−1073 544.6307	219 252 327 433	5×10^{-11}
10	−2428 264.8856	1256 378.6856	−10 704 624.457	24 415 176 279 909	1×10^{-9}
11	−30 987 268.4148	22 770 115.4386	−114 540 537.6	3×10^{16}	5×10^{-10}
12	−428 716 358.9148	440 685 490.5273	−1248 715 577	3×10^{18}	1×10^{-7}

Table 10. Evaluation of the bilinear form B_2 from (3.8) and (3.9) via J_i's.

d	J_{11}	J_{12}	J_{22}	JJ	$\lvert\frac{J_{12}}{J_{21}}-1\rvert$
5	80.6653	−483.0279	1388.5127	−121 311.0934	1×10^{-10}
6	611.2497	−3969.9773	12386.6137	−8189 405.1473	2×10^{-10}
7	5608.4168	−39 096.1569	134 642.4625	−773 378 434.5754	1×10^{-9}
8	60 626.5104	−449 322.1199	1721 581.0897	−97 516 913 089.4223	1×10^{-9}
9	758 310.8674	−5924 273.2959	25 329 030.7313	−158 897 345 947 79.6	1×10^{-9}
10	10 852 351.2386	−88 679 869.0076	423 309 818.7944	−3270 212 385 731 735	1×10^{-8}
11	176 804 567.641	−1500 253 955.9189	7990 965 776.4667	-8×10^{17}	1×10^{-7}
12	3286 852 523.1216	−28 762 231 494.6882	171 112 628 940.871	-3×10^{20}	1×10^{-6}

Table 11. Comparison of values of K_i's in $d=5$ between Chebyshev-collocation method and '`bvp4c`'. The boundary condition used here in both methods is $u(\infty)=0$.

$d=5$	K_{11}	K_{12}	K_{22}	KK	$\lvert K_{12}-K_{21}\rvert$
'cheby'	−42.3114	4.515	−490.2964	20724.7444	5×10^{-10}
'`bvp4c`'	−42.3114	4.515	−490.2966	20724.7515	3×10^{-05}

We use two methods to solve the equation (3.4): one is the Chebyshev collocation method; the other method is the matlab solver '`bvp4c`'. These two methods lead to basically the same results, for a comparison in dimension $d=5$ see table 11 (values of K_i's) and table 12 (values of J_i's). Since L_1 and L_2 are self-adjoint operators, the difference $\lvert\frac{K_{12}}{K_{21}}-1\rvert$, and the corresponding one for J's, is one way to check the numerical consistency, we list those values in the last columns of the tables 9 and 10; in tables 11 and 12 we list the differences $\lvert K_{12}-K_{21}\rvert$ and $\lvert J_{12}-J_{21}\rvert$, correspondingly.

We note that we use $u(\infty)=0$ boundary condition when computing the values of K's in table 9 as well as in table 11; moreover, in table 11 we provide results obtained by two methods for comparison purposes.

In the table 12 we show two different boundary conditions: $u(\infty)=0$ (first row with Chebyshev collocation method) and $u'(L)=0$ with Chebyshev collocation methods (second row) and with '`bvp4c`' from matlab (third row). This is for comparison of the results with lower dimensions, since it makes a difference in dimension four (though it does not influence the signs, thus, the conclusion of the spectral property), and it completely changes the results

Table 12. Comparison of values of J_i's for $d = 5$. Note that the boundary conditions affect the final results.

B.C.	J_{11}	J_{22}	J_{12}	JJ	$\lvert J_{12} - J_{21}\rvert$
$u(\infty) = 0$ by 'cheby'	80.6653	1388.5127	−483.0279	−121 311.0935	7×10^{-8}
$u'(L) = 0$ by 'cheby'	−114.8176	−4100.538	552.837	165 185.398	2×10^{-4}
$u'(L) = 0$ by 'bvp4c'	−114.8176	−4100.5315	552.8372	165 185.2598	2×10^{-3}

in dimension five (and higher). Therefore, starting from the dimension five and higher, we only use boundary condition as in the first row of table 11.

With these bilinear forms calculated, we reach the following proposition:

Proposition 3.5. *The bilinear form $B_1(f, f)$ is coercive on the space $\mathcal{U} = \{Q, Q_1\}^\perp$ and $\mathcal{U} \subseteq H_r^1$, where H_r^1 stands for the radial functions in H^1. The bilinear form $B_2(g,g)$ is coercive on the space $\mathcal{V} = \{Q_1, Q_2\}^\perp$ and $\mathcal{V} \subseteq H_r^1$. Therefore, the spectral property 1 holds in the functional space $\mathcal{U} \times \mathcal{V} \subseteq H_r^1 \times H_r^1$.*

Proof. We outline the key steps of the proof, we refer to [10, 29] or [42] for the details, as they are the same. Let us consider the form B_1 and recall from proposition 3.2 that the $\mathrm{ind}_{H_r^1}(B_1) = 2$. From the table 9 we have $K_{11} = B_1(U_1, U_1) < 0$. This suggests that U_1 is one of the negative spans of L_1 associated with B_1. Similarly, we have U_2 is the other negative span of L_1 associated to B_1, since $K_{22} < 0$. Moreover, the determinant $KK > 0$ suggests that the matrix from their linear combinations is negative definite, and thus, the decomposition is non-degenerate. In summary, since we exhibit two negative spans and $\mathrm{ind}(B_1) = 2$, the remaining spans, that are orthogonal to (U_1, U_2) in the sense of B_1, or equivalently, orthogonal to Q or Q_1 in L^2 sense, must generate the positive outcome, i.e. $B_1(f, f) > 0$ if $\langle f, Q\rangle = \langle f, Q_1\rangle = 0$.

Next, we consider the bilinear form B_2, while $J_{11} = B_2(Z_1, Z_1)$ and $J_{22} = B_2(Z_2, Z_2)$ generate the positive values, we check their linear combination $\bar{Z} = Z_1 + \alpha Z_2$ with $\alpha = -\frac{J_{12}}{J_{22}}$. This value comes from the fact that if we calculate the quadratic form, this constant gives the minimum value for the bilinear form. Moreover, $B_2(\bar{Z}, \bar{Z}) = C \cdot JJ$ for some constant $C > 0$, i.e. the value of the bilinear form has the same sign as the determinant. Thus, $JJ < 0$ suggests $B_2(\bar{Z}, \bar{Z}) < 0$ and $\bar{Z}$ lies on the negative span of L_2 as we desire. Therefore, any g, which is orthogonal to the direction $\bar{Z}$, i.e. $B_2(g, \bar{Z}) = 0$, or equivalently, $\langle g, Q_1\rangle = \langle g, Q_2\rangle = 0$, is orthogonal to (Z_1, Z_2), since $\bar{Z}$ is their linear combination, and consequently, we have $B_2(g,g) > 0$, which justifies the statement of proposition 3.5.

To make the argument rigorous, note that the functions f and g, considered above, are not in H_r^1 (from the proposition 3.4, we have $(1 + r^{d-2})f \in L^\infty(\mathbb{R}^d)$ and a similar requirement for g). We introduce an appropriate cut-off function and then take the limit. For further details, see [10, 29] or [42]. □

Finally, we provide details on the spectral property 2, where the orthogonal conditions for the second bilinear form can be changed to just one condition. We set $L_2 Z = Q$ and compute the quantity $\langle L_2 Z, Z\rangle$. Table 13 contains the values for the quantity $\langle L_2 Z, Z\rangle$ in dimensions two–six with two different boundary conditions, and then in dimensions 7–12 with $u(\infty) = 0$.

Remark 3.3. Since by proposition 3.2 the index of L_2 is one, arguing as in proposition 3.5 and incorporating the results from table 13, we obtain that the spectral property holds for L_2 only with one condition: $\langle Q, g\rangle = 0$, which proves theorem 1.2, and thus, validates the spec-

Table 13. Value of $\langle L_2 Z, Z\rangle$ for different dimensions, where $L_2 Z = Q$.

Boundary conditions	d	2	3	4	5	6
$u'(L) = 0$	$\langle L_2 Z, Z\rangle$	−2.9513	−4.8101	39.6029	−173.4202	−14 058.3264
$u(\infty) = 0$	$\langle L_2 Z, Z\rangle$	NA	−6.7563	−23.3181	−107.8715	−623.5943
d	7	8	9	10	11	12
$\langle L_2 Z, Z\rangle, u(\infty) = 0$	−4290.4717	−33763.4	−291 711	−2604 677	−20 638 152	−33 716 967

tral property 2 in the radial case. For completeness, we include details in the general case in theorem 3.6.

3.2. The non-radial case

To study the non-radial case, we rewrite our operators in the form of spherical harmonics, i.e.

$$L_{1,2}^{(k)} = -\partial_{rr} - \frac{d-1}{r}\partial_r + V_{1,2}(r) + \frac{k(k+d-2)}{r^2}, \quad k = 0, 1, 2, ... \tag{3.10}$$

The notation $L_{1,2}^{(k)}$ and $B_{1,2}^{(k)}$ will stand for the kth spherical harmonics. When $k = 0$, it is simply the radial case, which we already discussed in section 3.1. For $k > 0$ the bilinear forms $B_{1,2}^{(k)}$ have the same properties as $L_{1,2}^{(k)}$, similar to the case $k = 0$ (see [10, 40] and [29]). We first study indices of the kth bilinear forms.

Proposition 3.6 (Indices in the non-radial case). *The index of the bilinear form* $\mathrm{ind}(B_{1,2}^{(k)})$ *equals the number of zeros of the IVP problem, counting from* $r > 0$*:*

$$\begin{cases} L_{1,2}^{(k)} U^{(k)} = 0, \\ \lim_{r\to 0} \frac{U^{(k)}(r)}{r^k} = 1, \\ \lim_{r\to 0} \frac{\mathrm{d}}{\mathrm{d}r} \frac{U^{(k)}(r)}{r^k} = 0. \end{cases} \tag{3.11}$$

Numerical calculations show that for $d = 4, 5, 6, 7, 8, 9, 10$*, we have*

$$\mathrm{ind}(L_1^{(1)}) = 1, \quad \mathrm{ind}(L_1^{(2)}) = 0, \quad \mathrm{ind}(L_2^{(1)}) = 0.$$

Consequently,

$$\mathrm{ind}_{H^1}(B_1^{(1)}) = 1, \quad \mathrm{ind}_{H^1}(B_1^{(2)}) = 0, \quad \mathrm{ind}_{H^1}(B_2^{(1)}) = 0.$$

For $d = 11, 12$*, we get*

$$\mathrm{ind}(L_1^{(1)}) = 1, \quad \mathrm{ind}(L_1^{(2)}) = 1, \quad \mathrm{ind}(L_1^{(3)}) = 0,$$

$$\mathrm{ind}(L_2^{(1)}) = 1, \quad \mathrm{ind}(L_2^{(2)}) = 0,$$

and consequently,

$$\mathrm{ind}_{H^1}(B_1^{(1)}) = 1, \quad \mathrm{ind}_{H^1}(B_1^{(2)}) = 1, \quad ind_{H^1}(B_1^{(3)}) = 0.$$

$$\mathrm{ind}_{H^1}(B_2^{(1)}) = 1, \quad \mathrm{ind}_{H^1}(B_2^{(2)}) = 0.$$

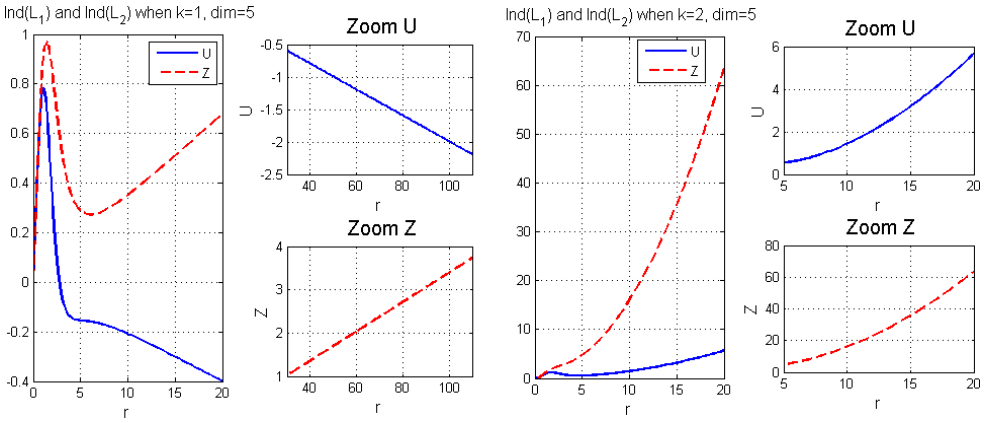

Figure 7. Solutions of (3.11) in $d = 5$. Numerical justification of the proposition 3.6. Left figure is the for $k = 1$ and right figure is for $k = 2$. The blue line shows the behaviors of U from $L_1^{(k)}U = 0$ and the red line shows the behaviors of Z from $L_2^{(k)}Z = 0$. To the right of each plot are zooms of the tails for U and Z. One can see the tails of U and Z increase or decrease with a rate r^k, which justifies the asymptotic behavior in (3.14).

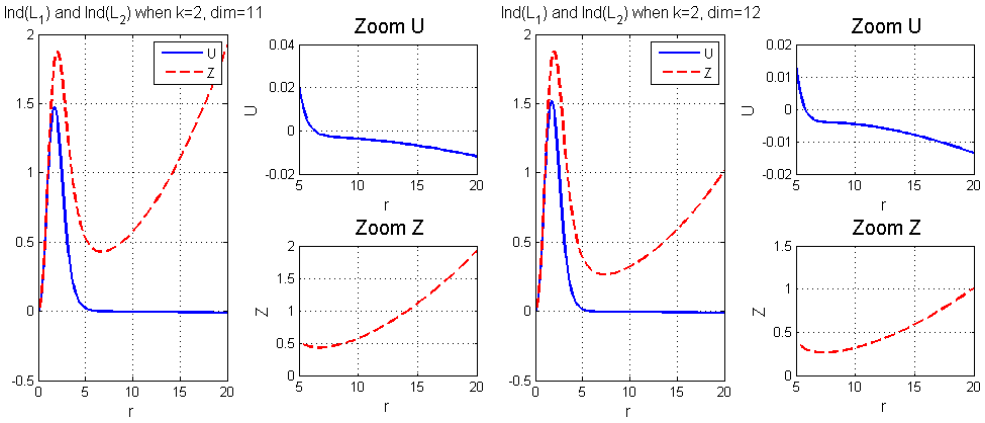

Figure 8. Solutions of (3.11) in $d = 11$ (left) and $d = 12$ (right), or numerical justification of the proposition 3.6. The blue line shows the behaviors of U from $L_1^{(2)}U = 0$ and the red line shows the behaviors of Z from $L_2^{(2)}Z = 0$. To the right of each plot are zooms of the tails for U and Z. One can see U and Z increase or decrease with a quadratic rate. This justifies the asymptotic behavior in (3.14) for $k = 2$.

This proposition is obtained from the numerical solutions of the IVP in (3.11) in the corresponding cases, see figure 7 as an example in the case $d = 5$. Figures 8 and 9 show the solution of (3.11) in cases $d = 11, 12$ and $k = 2, 3$, since they are different from the cases $d = 5, \cdots, 10$. Here, U stands for the solution of $L_1^{(k)}$, and Z for $L_2^{(k)}$.

In this non-radial case, in our numerical simulations, we want to get rid of the limit terms in the boundary conditions. We use the approach from [29]: let $U^{(k)}(r) = r^k \tilde{U}^{(k)}(r)$, then the operator $L_i^{(k)}$ becomes

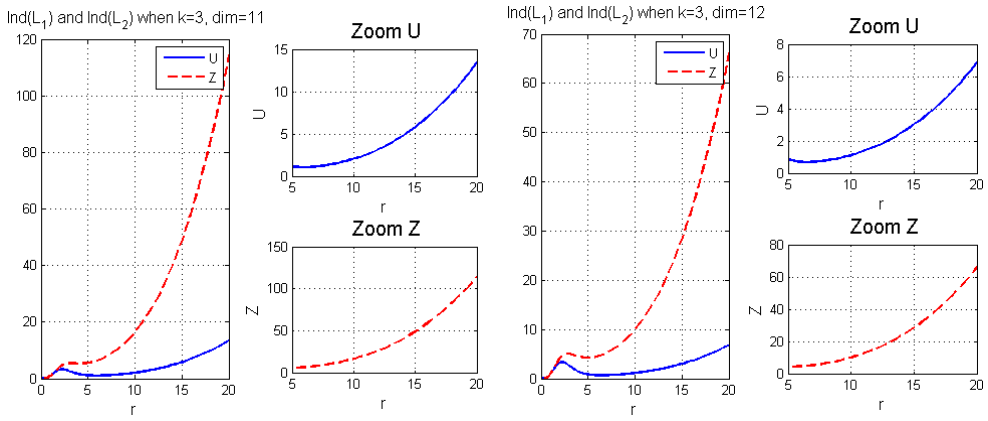

Figure 9. Solutions of (3.11) in $d = 11$ (left) and $d = 12$ (right), or numerical justification of the proposition 3.6. The blue line shows the behaviors of U from $L_1^{(3)}U = 0$ and the red line shows the behaviors of Z from $L_2^{(3)}Z = 0$. To the right of each plot are zooms of the tails for U and Z. One can see U and Z increase or decrease with a cubic rate. This justifies the asymptotic behavior in (3.14) for $k = 3$.

$$\tilde{L}_{1,2}^{(k)} = \partial_{rr} - \frac{d-1+2k}{r}\partial_r + V_{1,2}. \tag{3.12}$$

We rewrite (3.11) as follows

$$\begin{cases} r^k\left(-\partial_{rr}\tilde{U} - \frac{d-1+2k}{r}\partial_r\tilde{U} + V_{1,2}(r)\tilde{U}\right) = 0 \\ \tilde{U}(0) = 1, \quad \tilde{U}_r(0) = 0. \end{cases} \tag{3.13}$$

The IVP (3.13) can be solved by matlab solver '`ode45`'. Then the solution U can be reconstructed by $U(r) = r^k\tilde{U}(r)$. From [29, section3], it follows that $U(r)$ satisfies the asymptotic behavior for $r \gg 1$

$$U \approx C_1 r^k + C_2 r^{2-d-k}. \tag{3.14}$$

This indicates that for $r \gg 1$, $U(r)$ either grows or decays with a polynomial rate r^k. Consequently, no more zeros will occur. We stop calculations once we see such polynomial increase or decrease.

The following property ([40], also see [10, 29]) shows that once we found some k_0 such that $\mathrm{ind}(L_{1,2}^{(k_0)}) = 0$, we can stop the calculation. This avoids checking infinitely many k's.

Proposition 3.7. *The index is monotonic with respect to k, that is,*

$$\mathrm{ind}(B_{1,2}^{(k+1)}) \leqslant \mathrm{ind}(B_{1,2}^{(k)}).$$

Moreover, the uniqueness and stability of the indices of the bilinear forms $B_{1,2}$ can also be extended to the non-radial case:

Proposition 3.8 (Stability, [10, 29]). *For the operators $L_{1,2}^{(k)}$ defined in (3.10), there exists a universal constant $\delta_0 > 0$, sufficiently small, such that for the perturbed operators*

$$\bar{L}_{1,2}^{(k)} = L_{1,2}^{(k)} - \delta_0 \mathrm{e}^{-|x|},$$

Table 14. Values of $K_{11}^{(1)}$ corresponding to the form $B_1^{(1)}$.

d	5	6	7	8
$K_{11}^{(1)}$	−338.0072	−2514.4344	−21 858.3993	−216 907.232
d	9	10	11	12
$K_{11}^{(1)}$	−2409 681.326	−29 422 347	−386 097 788.7178	−5238 134 702.1673

the associated bilinear forms are stable:

$$\mathrm{ind}_{H^1}(\bar{B}_{1,2}^{(k)}) = \mathrm{ind}_{H^1}(B_{1,2}^{(k)}).$$

Proposition 3.9 (Invertibility, [10, 29]). *Let $d \in [5, 12]$ and $f \in C_{loc}^0(\mathbb{R}^d)$ with radial symmetry and $|f(r)| \leqslant \mathrm{e}^{-Cr}$. Then there exists a unique radial solution to*

$$L_{1,2}^{(k)} u = f \quad \textit{with } (1 + r^{d-2+k})u \in L^\infty(\mathbb{R}^d).$$

Similar to the radial case, we list the numerical values of the bilinear forms, needed to prove the spectral properties for the non-radial case.

Definition 3.4 (Numerical computations for the bilinear form). Let the operators $L_i^{(k)}$, $i = 1, 2$, solve the linear BVP

$$\begin{cases} L_{1,2}^{(k)} u = f, \\ u_r(0) = 0, \quad u(\infty) = 0. \end{cases} \tag{3.15}$$

Define

$$L_1^{(1)} U_1^{(1)} = rQ, \quad L_2^{(1)} Z_1^{(1)} = Q_r; \tag{3.16}$$

$$L_1^{(2)} U_1^{(2)} = rQ \tag{3.17}$$

and denote the following constants as values of the bilinear forms

$$K_{11}^{(1)} = B_1^{(1)}(U_1^{(1)}, U_1^{(1)}), \quad J_{11}^{(1)} = B_2^{(1)}(Z_1^{(1)}, Z_1^{(1)}), \quad K_{11}^{(2)} = B_1^{(2)}(U_1^{(2)}, U_1^{(2)}). \tag{3.18}$$

The values of $K_{ij}^{(k)}$'s and $J_{ij}^{(k)}$'s are listed in tables 14–16.

The values of these bilinear forms are computed by Chebyshev collocation method with $N = 1025$ collocation points on the interval $L = 100$. The artificial boundary condition is constructed in a similar way as in the previous section 3.1 to approximate $u(\infty) = 0$, see also appendix C for details on artificial boundary condition.

We are now ready to establish both spectral properties.

Theorem 3.5. *Let the space $\mathcal{U} = \{Q, Q_1, x_i Q\}^\perp \subseteq H^1$, and the space $\mathcal{V} = \{Q_1, Q_2, Q_{x_i}\}^\perp \subseteq H^1$, where $i = 1, 2, \cdots, d$. In the dimensions $d \leqslant 10$, the spectral property 1 holds on the given subspace $\mathcal{U} \times \mathcal{V} \subseteq H^1 \times H^1$. In the dimension $d = 11$ or $d = 12$, the spectral property 1 holds only on the given subspace $\mathcal{U} \times \mathcal{V} \subseteq H_r^1 \times H_r^1$. It is indecisive in the non-radial case.*

Proof. We only outline the main idea, as it follows the proof in [10] and [29]. For $d \leqslant 10$, $\mathrm{ind}(L_1^{(1)}) = 1$, and we see $K_{11} < 0$ from table 14. Thus, $U_1^{(1)}$ generates the negative span. For any $f \in \{U_1^{(1)}\}^\perp$ in the $B_1^{(1)}$ sense, $B_1^{(1)}(f, f) > 0$. For $L_1^{(2)}$ and $L_2^{(1)}$, $\mathrm{ind}(L_1^{(2)}) = \mathrm{ind}(L_2^{(1)}) = 0$,

Table 15. Values of $J_{11}^{(1)}$ corresponding to the form $B_2^{(1)}$.

d	5	6	7	8
$J_{11}^{(1)}$	689.5337	6433.9656	73 995.9077	1055 378.5046
d	9	10	11	12
$J_{11}^{(1)}$	19 767 639.0831	648 419 143	−17491 047 782	−69 767 861 282

Table 16. Values of $K_{11}^{(2)}$ corresponding to the form $B_1^{(2)}$.

d	11	12
$K_{11}^{(2)}$	52 218 994 506 811	34 912 990 629 971 056

thus $B_1^{(2)}$ and $B_2^{(1)}$ are coercive. The coercivity of both B_1 and B_2 implies the spectral property in the given space $\mathcal{U} \times \mathcal{V}$. We need to note that f and g may not necessarily in H_r^1, since from the proposition 3.4, $(1 + r^{d-2+k})f \in L^\infty(\mathbb{R}^d)$ and the same for g. Similar to the radial case we discuss above, we need to introduce an appropriate cut-off function and then take the limit as what the authors did in [10, 29] or [42].

For the case $d = 11$ or $d = 12$. $B_1^{(1)}$ and $B_2^{(1)}$ are coercive on the subspace of H_r^1 that satisfies the orthogonal conditions from $K_{11} < 0$ and $J_{11} < 0$. However, when $k = 2$, the index of $L_1^{(2)}$ is still one and we get the positive values from the bilinear forms (see table 16). Thus, the coercivity of $B_1^{(2)}$ becomes indecisive. Hence, with current computations, we can only show the spectral property under the radial assumption for $d = 11$ or $d = 12$. □

Theorem 3.6. *Let the space $\mathcal{U} = \{Q, Q_1, x_i Q\}^\perp \subseteq H^1$, and the space $\mathcal{V} = \{Q, Q_{x_i}\}^\perp \subseteq H^1$, where $i = 1, 2, \cdots, d$. In the dimensions $d \leqslant 10$, the spectral property 2 holds on the given subspace $\mathcal{U} \times \mathcal{V} \subseteq H^1 \times H^1$. In the dimension $d = 11$ or $d = 12$, the spectral property 2 holds only on the given subspace $\mathcal{U} \times \mathcal{V} \subseteq H_r^1 \times H_r^1$. It is indecisive for the non-radial case.*

Proof. The argument follows the proof of theorem 3.5. From table 13, one can see that the span of $\tilde{Z}$, where $L_2\tilde{Z} = Q$, is negative. Combining with the fact that $\mathrm{Ind}(L_2^{(0)}) = 1$, we conclude that $\tilde{Z}$ is the only negative span we have. Therefore, the coercivity of $B_2^{(0)}$ is reached on the subspace orthogonal to Q. For the non-radial case, the proof is the same as the orthogonal conditions to extend to the nonradial setting are the same as in the theorem 3.5, and thus, finishing the proof. □

Remark 3.7. In the dimensions $d = 11$ and $d = 12$, $\mathrm{ind}(L_2^{(1)}) = 1$ instead of the zero index, which is not what we obtained in the lower dimensions. We double checked this with the standard 4th order explicit Runge–Kutta method (RK4), taking the step size $h = 0.001$ in obtaining solutions to (3.11). This led to the same results as in the above calculations via the matlab solver '`ode45`'. Table 15 shows the negative values for $J_{11}^{(1)}$ in $d = 11$ and $d = 12$, which also suggests that the index of $L_2^{(1)}$ is not zero in those dimensions. We also numerically calculated the negative eigenvalue of $L_2^{(1)}$: $\lambda = -0.01403$ in the dimension $d = 11$, and $\lambda = -0.0560$ in the dimension $d = 12$. This can be compared with the situation of the index of $L_1^{(0)}$ in the dimensions $d = 2$ and $d = 3$, $\mathrm{ind}(L_1^{(0)}) = 1$ when $d = 2$ but $\mathrm{ind}(L_1^{(0)}) = 2$ when $d = 3$, see [10] and [11].

4. Conclusions

In this paper we first discussed direct numerical simulations of the generic blow-up solutions in the L^2-critical NLS equation in higher dimensions ($d = 4, ..., 12$) under the radial symmetry assumption. Our results show that the 'log–log' law is universal for all L^2-critical NLS equations (at least up to $d = 12$). Secondly, we investigated the spectral property 1 in higher dimensions, which is the essential part of the analytical proof of the 'log–log' regime for the cases when the mass of the negative energy initial data is slightly above the mass of Q, the corresponding ground state Q for the given dimension and nonlinearity. We confirm that the spectral property 1 (as well as a modified version of it) holds from $d = 5$ to $d = 10$ in a general case, and for $d = 11$ and $d = 12$, at least, in the radial case. Therefore, we conclude that the 'log–log' blow-up regime is the stable blow-up regime in $d \leqslant 10$ and radially stable in $d \leqslant 12$.

Acknowledgments

The authors would like to thank Gideon Simpson for his visit to GWU and posing some of the questions addressed in this paper as well as for helpful discussions on this topic. The authors are grateful for the fruitful discussions, the initial guidance for numerics and comments on the initial draft of the paper to Pavel Lushnikov, who also visited GWU in April 2017, and whose trip was partially supported by GWIMS. SR would like to thank Pierre Raphaël for bringing to her attention [11] and for posing the question about the orthogonality condition (1.18). KY and YZ would like to acknowledge Yongyong Cai, who hosted their visit to the Computational Science Research Center (CSRC) in Beijing during Summer 2017. SR was partially supported by the NSF CAREER grant DMS-1151618 as well as part of the KY's graduate research fellowship to work on this project came from the above grant. YZ was partially supported by the Simons Foundation through grant no. 357963.

Appendix A. Justification of 'log–log' corrections in $d = 6, ..., 12$

Here, we list different functional fittings $F(s)$ for the correction term in the blow-up rate (2.25) in the dimensions $d = 6, ..., 12$. For dimensions $d = 6$ and 7 we list our computations for ρ_i with $F(s) = 1, \left(\ln \frac{1}{s}\right)^{\gamma}$, $\gamma = 0.25, 0.2, 0.15$ and $\ln \ln \frac{1}{s}$ in tables A1 and A2. One can observe that log–log shows better stabilization in the approximation of the power ρ_i, though, the other approximation seem to reach 0.5 at some time period and stay there for a while, but then keep decreasing away from it.

We also give l^2 discrepancy ϵ_i results (for the last three steps from $j_0 = 7$ to $i = 9$) in table A3 for both $d = 6, 7$. It seems that the smallest error is given by the power $\gamma = 0.2$, which can be explained similarly as in the dimension $d = 4$ (during the studied time interval, this functional approximation decreases down to 0.5, but then it will continue decreasing). Similar comments can be made about other powers of γ.

For higher dimensions, for brevity, we list $F(s) = 1$ and $F(s) = \ln \ln \frac{1}{s}$ results, see tables A4–A8 for dimensions $d = 8, 9, 10, 11, 12$, correspondingly.

Table A1. Comparison of the different functional forms $F(s)$ for the correction term in $d = 6$. '$\frac{1}{L(t)}$ range' means the values $\frac{1}{L(t_i)} \sim \frac{1}{L(t_{i+1})}$.

	The fitting power ρ_i from different corrections $F(s)$					
i	$\frac{1}{L(t)}$ range	1	$(\ln \frac{1}{s})^{0.25}$	$(\ln \frac{1}{s})^{0.2}$	$(\ln \frac{1}{s})^{0.15}$	$\ln \ln \frac{1}{s}$
0	$2 \times 10^4 \sim 7 \times 10^5$	0.5104	0.5010	0.5029	0.5048	0.4959
1	$2 \times 10^4 \sim 7 \times 10^5$	0.5064	0.5003	0.5015	0.5027	0.4984
2	$7 \times 10^5 \sim 2 \times 10^7$	0.5045	0.5000	0.5009	0.5018	0.4990
3	$2 \times 10^7 \sim 4 \times 10^8$	0.5035	0.4998	0.5005	0.5013	0.4993
4	$4 \times 10^8 \sim 8 \times 10^9$	0.5028	0.4997	0.5003	0.5009	0.4994
5	$8 \times 10^9 \sim 1 \times 10^{11}$	0.5024	0.4996	0.5002	0.5007	0.4995
6	$1 \times 10^{11} \sim 3 \times 10^{12}$	0.5020	0.4996	0.5001	0.5006	0.4996
7	$3 \times 10^{12} \sim 4 \times 10^{13}$	0.5018	0.4996	0.5000	0.5005	0.4996
8	$4 \times 10^{13} \sim 6 \times 10^{14}$	0.5016	0.4996	0.5000	0.5004	0.4997
9	$6 \times 10^{14} \sim 9 \times 10^{15}$	0.5014	0.4996	0.5000	0.5003	0.4997

Table A2. Comparison of the different functional forms $F(s)$ for the correction term in $d = 7$. '$\frac{1}{L(t)}$ range' means the values $\frac{1}{L(t_i)} \sim \frac{1}{L(t_{i+1})}$.

	The fitting power ρ_i from different corrections $F(s)$					
i	$\frac{1}{L(t)}$ range	1	$(\ln \frac{1}{s})^{0.25}$	$(\ln \frac{1}{s})^{0.2}$	$(\ln \frac{1}{s})^{0.15}$	$\ln \ln \frac{1}{s}$
0	$2 \times 10^2 \sim 1 \times 10^4$	0.5104	0.4995	0.5016	0.5038	0.4924
1	$1 \times 10^4 \sim 4 \times 10^5$	0.5063	0.4997	0.5010	0.5023	0.4973
2	$4 \times 10^5 \sim 9 \times 10^6$	0.5044	0.4996	0.5006	0.5015	0.4985
3	$9 \times 10^6 \sim 2 \times 10^8$	0.5034	0.4996	0.5003	0.5011	0.4990
4	$2 \times 10^8 \sim 5 \times 10^9$	0.5028	0.4995	0.5002	0.5008	0.4992
5	$5 \times 10^9 \sim 1 \times 10^{11}$	0.5023	0.4995	0.5001	0.5006	0.4994
6	$1 \times 10^{11} \sim 2 \times 10^{12}$	0.5020	0.4995	0.5000	0.5005	0.4995
7	$2 \times 10^{12} \sim 3 \times 10^{13}$	0.5017	0.4995	0.5000	0.5004	0.4995
8	$3 \times 10^{13} \sim 5 \times 10^{14}$	0.5015	0.4995	0.4999	0.5003	0.4996
9	$5 \times 10^{14} \sim 9 \times 10^{15}$	0.5014	0.4995	0.4999	0.5003	0.4996

Table A3. The l^2 discrepancy ϵ_i calculated from $j_0 = 7$ to $i = 9$ for the fittings given in tables A1–A2 in $d = 6$ and $d = 7$.

d	$F(s) = 1$	$F(s) = (\ln \frac{1}{s})^{0.25}$	$F(s) = (\ln \frac{1}{s})^{0.2}$	$F(s) = (\ln \frac{1}{s})^{0.15}$	$F(s) = \ln \ln \frac{1}{s}$
6	0.0017	4.04×10^{-4}	5.56×10^{-5}	4.51×10^{-4}	3.71×10^{-4}
7	0.0017	4.76×10^{-4}	6.18×10^{-5}	3.88×10^{-4}	4.50×10^{-4}

We conclude this section with providing the l^2 discrepancy error (computed for the last three steps) for dimensions $d = 8, ..., 12$ in table A9. The error ϵ_i stays on the same order $\sim 10^{-4}$ as in all previous dimensions.

Table A4. Comparison of the functional fitting in $d = 8$.

i	$\frac{1}{L(t)}$ range	ρ_i from $F(s) = 1$	ρ_i from $F(s) = \ln\ln\frac{1}{s}$
0	$7 \times 10^3 \sim 3 \times 10^5$	0.5069	0.4974
1	$3 \times 10^5 \sim 8 \times 10^6$	0.5047	0.4986
2	$8 \times 10^6 \sim 2 \times 10^8$	0.5035	0.4991
3	$2 \times 10^8 \sim 5 \times 10^9$	0.5028	0.4993
4	$5 \times 10^9 \sim 1 \times 10^{11}$	0.5024	0.4994
5	$1 \times 10^{11} \sim 2 \times 10^{12}$	0.5020	0.4995
6	$2 \times 10^{12} \sim 4 \times 10^{13}$	0.5017	0.4996
7	$4 \times 10^{13} \sim 8 \times 10^{14}$	0.5015	0.4996
8	$8 \times 10^{14} \sim 1 \times 10^{16}$	0.5014	0.4996

Table A5. Comparison of the functional fitting in $d = 9$.

i	$\frac{1}{L(t)}$ range	ρ_i from $F(s) = 1$	ρ_i from $F(s) = \ln\ln\frac{1}{s}$
0	$4 \times 10^3 \sim 2 \times 10^5$	0.5069	0.4968
1	$2 \times 10^5 \sim 7 \times 10^6$	0.5047	0.4983
2	$7 \times 10^6 \sim 2 \times 10^8$	0.5035	0.4989
3	$2 \times 10^8 \sim 5 \times 10^9$	0.5028	0.4992
4	$5 \times 10^9 \sim 1 \times 10^{11}$	0.5023	0.4993
5	$1 \times 10^{11} \sim 2 \times 10^{12}$	0.5020	0.4994
6	$2 \times 10^{12} \sim 5 \times 10^{13}$	0.5017	0.4995
7	$5 \times 10^{13} \sim 9 \times 10^{14}$	0.5015	0.4996
8	$9 \times 10^{14} \sim 2 \times 10^{16}$	0.5013	0.4996

Table A6. Comparison of the functional fitting in $d = 10$.

i	$\frac{1}{L(t)}$ range	ρ_i from $F(s) = 1$	ρ_i from $F(s) = \ln\ln\frac{1}{s}$
0	$3 \times 10^3 \sim 2 \times 10^5$	0.5065	0.4959
1	$2 \times 10^5 \sim 5 \times 10^6$	0.5044	0.4979
2	$5 \times 10^6 \sim 2 \times 10^8$	0.5033	0.4986
3	$2 \times 10^8 \sim 4 \times 10^9$	0.5026	0.4990
4	$4 \times 10^9 \sim 1 \times 10^{11}$	0.5022	0.4992
5	$1 \times 10^{11} \sim 2 \times 10^{12}$	0.5019	0.4993
6	$2 \times 10^{12} \sim 5 \times 10^{13}$	0.5016	0.4994
7	$5 \times 10^{13} \sim 9 \times 10^{14}$	0.5014	0.4995
8	$9 \times 10^{14} \sim 2 \times 10^{16}$	0.5013	0.4996

Appendix B. Artificial boundary conditions

The BVP problem (3.4) and (3.15) involves the boundary condition $u(\infty) = 0$. We use the approach in [29] to construct the artificial boundary condition to approximate $u(\infty) = 0$.

As $V_{1,2}$ and f decay exponentially fast, as it was discussed before, for $r \gg 1$ the solutions of (3.15) converge to their linear flows:

Table A7. Comparison of the functional fitting in $d = 11$.

i	$\frac{1}{L(t)}$ range	ρ_i from $F(s) = 1$	ρ_i from $F(s) = \ln\ln\frac{1}{s}$
0	$2 \times 10^3 \sim 1 \times 10^5$	0.5060	0.4945
1	$1 \times 10^5 \sim 4 \times 10^6$	0.5041	0.4972
2	$4 \times 10^6 \sim 1 \times 10^8$	0.5031	0.4982
3	$1 \times 10^8 \sim 3 \times 10^9$	0.5025	0.4987
4	$3 \times 10^9 \sim 7 \times 10^{10}$	0.5021	0.4990
5	$7 \times 10^{10} \sim 2 \times 10^{12}$	0.5018	0.4992
6	$2 \times 10^{12} \sim 4 \times 10^{13}$	0.5015	0.4993
7	$4 \times 10^{13} \sim 8 \times 10^{14}$	0.5014	0.4994
8	$8 \times 10^{14} \sim 2 \times 10^{16}$	0.5012	0.4995

Table A8. Comparison of the functional fitting in $d = 12$.

i	$\frac{1}{L(t)}$ range	ρ_i from $F(s) = 1$	ρ_i from $F(s) = \ln\ln\frac{1}{s}$
0	$2 \times 10^3 \sim 9 \times 10^4$	0.5059	0.4940
1	$9 \times 10^4 \sim 3 \times 10^6$	0.5040	0.4970
2	$3 \times 10^6 \sim 1 \times 10^8$	0.5030	0.4981
3	$1 \times 10^8 \sim 3 \times 10^9$	0.5024	0.4987
4	$3 \times 10^9 \sim 8 \times 10^{10}$	0.5020	0.4990
5	$8 \times 10^{10} \sim 2 \times 10^{12}$	0.5017	0.4992
6	$2 \times 10^{12} \sim 4 \times 10^{13}$	0.5015	0.4993
7	$4 \times 10^{13} \sim 1 \times 10^{15}$	0.5014	0.4994
8	$1 \times 10^{15} \sim 2 \times 10^{16}$	0.5012	0.4995

Table A9. The l^2 discrepancy ϵ_i calculated from $j_0 = 7$ to $i = 9$ for the fittings given in tables A4–A8 in $d = 8, 9, 10, 11, 12$.

d	$F(s) = 1$	$F(s) = \ln\ln\frac{1}{s}$
8	0.0017	4.23×10^{-4}
9	0.0016	4.69×10^{-4}
10	0.0016	5.43×10^{-4}
11	0.0015	6.48×10^{-4}
12	0.0014	6.87×10^{-4}

$$-\partial_{rr}u - \frac{d-1+2k}{r}\partial_r u = 0, \quad r \gg 1. \tag{B.1}$$

This equation has the explicit solution

$$u = \frac{C_1}{r^{d-2+k}} + C_2 := C_1\phi_1 + C_2\phi_2, \tag{B.2}$$

where $\phi_1 = \frac{1}{r^{d-2+k}}$ and $\phi_2 = 1$. Since $u(\infty) = 0$, only span ϕ_1 remains. Consequently, at $r = L$, the solution to (3.15) must be linearly dependent on ϕ_1. Therefore, their Wronskian should equal to 0, i.e.

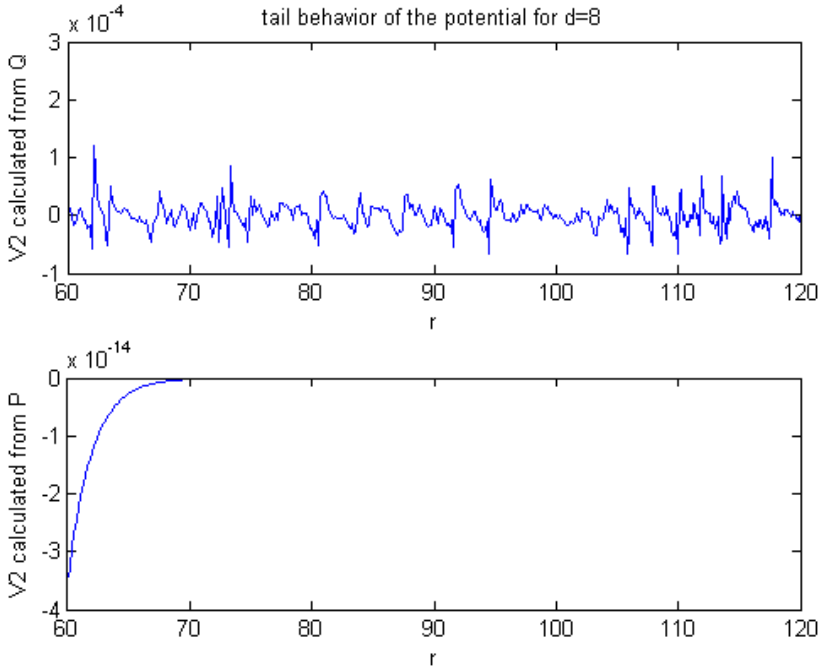

Figure C1. Upper: the value of V_2 calculated directly from Q; lower: V_2 obtained from P. Our method calculating $V2$ from P completely avoids oscillations.

$$\det \begin{pmatrix} u(L) & \phi_1(L) \\ u_r(L) & \phi_1'(L) \end{pmatrix} = 0, \tag{B.3}$$

which is

$$u(L) + \frac{L}{d-2+2k} u_r(L) = 0. \tag{B.4}$$

Therefore, the boundary condition $u(\infty) = 0$ is substituted by $u(L) + \frac{L}{d-2+2k} u_r(L) = 0$ at the length of the interval $r = L$.

Appendix C. Computation of the potentials V_1 and V_2

When $d \geqslant 5$, the term $Q^{\frac{4}{d}-1}$ in $V_{1,2}$ has the negative power. We rewrite it as follows, for example for V_2

$$V_2 = \frac{2}{d} Q^{\frac{4}{d}} r \frac{Q_r}{Q}.$$

Recall that the ground state Q decays with the rate $Q \sim r^{-\frac{d-1}{2}} \mathrm{e}^{-r}$ for $r \gg 1$ (e.g. see [29]). Consequently, $Q_r \sim -Q$ and only differs by a polynomial power, and V_2 decays with an exponential rate $V_2 \sim \mathrm{e}^{-\frac{4}{d}r}$ for $r \gg 1$. However, if we compute the V_2 from (1.08), instead of keep decreasing, the potential term V_2 becomes oscillating at the magnitude 10^{-4} when $r \geqslant 40$ in $d = 8$. This fails to describe the 'fast decay' property of the potential terms and may cause trouble in the process of finding the index of $L_{1,2}^{(k)}$ (according to [40], $L_{1,2}$ has infinitely many negative eigenvalues if the potential decays slower than $\frac{1}{r^2}$). In fact, this issue comes from the

Table C1. Comparison of the quantities obtained in two different ways, where $\tilde{V}_2 = \frac{2}{d} P^{\frac{4}{d}} r \left(\frac{P_r}{P} - 1\right) \mathrm{e}^{-\frac{4}{d}}$. We set $L = 100$, $N = 1024$.

d	5	6	7	8	9	10	11	12
$\|Q - P\mathrm{e}^{-r}\|_\infty$	4×10^{-09}	5×10^{-09}	7×10^{-09}	1×10^{-8}	3×10^{-08}	4×10^{-7}	4×10^{-05}	6×10^{-3}
$\|V_2 - \tilde{V}_2\|_\infty$	1×10^{-09}	2×10^{-07}	8×10^{-06}	1×10^{-4}	1×10^{-3}	6×10^{-3}	0.0491	0.09

numerical calculation of the ground state Q. When we compute the ground state Q, the Q itself stops decreasing when it reaches the magnitude of 10^{-14}, since it is less than the tolerance we set for the fixed point iteration and it approaches the machine accuracy. Nevertheless, $(10^{-14})^{\frac{4}{d}}$ could be a relatively large number, especially when the dimension d is large, say $d \geqslant 8$.

While we cannot find a way to refine the numerical method for finding the ground state Q as it is below our tolerance and approaching the machine accuracy, we come up with an alternative way to compute the potential terms, say V_2. We outline it next.

Consider the function

$$P(r) = Q(r)\,\mathrm{e}^r. \tag{C.1}$$

Where P decays with a polynomial rate $r^{-\frac{d-1}{2}}$, since $Q \sim r^{-\frac{d-1}{2}} \mathrm{e}^{-r}$ for $r \gg 1$. Then, a straightforward calculation gives us

$$V_2 = \frac{2}{d} P^{\frac{4}{d}} r \left(\frac{P_r}{P} - 1\right) \mathrm{e}^{-\frac{4}{d}}. \tag{C.2}$$

This implies that if we find the profile of P, which decays polynomially, then P can not be too small for $r \gg 1$. Moreover, the last term $\mathrm{e}^{-\frac{4}{d}}$ describes an exponential decay for the potential V_2.

Putting the expression $P(r) = Q(r)e^r$ into the ground state equation (1.5), we have

$$\begin{cases} P_{rr} - 2P_r + \frac{d-1}{r}(P_r - P) + P^{\frac{4}{d}+1}\mathrm{e}^{-\frac{4}{d}r} = 0, & (P > 0), \\ P_r(0) - P(0) = 0, \\ P(\infty) = 0. \end{cases} \tag{C.3}$$

We can construct the artificial boundary condition to approximate $P(\infty) = 0$ the same way as for $L_{1,2}u = f$. As described in section 3, the linear flow of the equation (C.3) gives us

$$P_{rr} - 2P_r + \frac{d-1}{r}(P_r - P) = 0. \tag{C.4}$$

The solutions of the free equation decay with the leading order $P \sim r^{-\frac{d-1}{2}}$. Therefore, we can construct the artificial boundary condition at $r = L$:

$$\det \begin{pmatrix} P(r) & r^{-\frac{d-1}{2}} \\ P_r(r) & -\frac{d-1}{2} r^{-\frac{d+1}{2}} \end{pmatrix} = 0, \tag{C.5}$$

i.e.

$$P + \frac{2L}{d-1} P_r = 0. \tag{C.6}$$

We use the Chebyshev differential matrices to discretize the first and second derivatives P_r and P_{rr}, then the discretized equation (C.3) changes to the nonlinear system

Table D1. Comparison of the bilinear forms for K_{ij}'s and J_{ij}'s by using different boundary conditions. This is for the case $d = 2$.

Boundary conditions	K_{11}	K_{22}	K_{12}	J_{11}	J_{22}	J_{12}
In [10, pp 7–8], $u'(L) = 0$	−0.65	*NA*	*NA*	0.9969	12.4211	−4.4095
$u'(L) = 0$ from 'cheby'	−0.65343	16.0778	−1.3054	1.0058	12.7804	−4.4705
$u'(L) = 0$ from '`bvp4c`'	−0.65344	16.0778	−1.3054	1.0058	12.7804	−4.4705

Table D2. Comparison of the bilinear forms for K_{ij}'s and J_{ij}'s by using different boundary conditions. This is for the case $d = 3$.

Boundary conditions	K_{11}	K_{22}	K_{12}	J_{11}	J_{22}	J_{12}
In [10, pp 7–8], $u'(L) = 0$	−2.1	*NA*	*NA*	5.9141	100.36881	−28.0500
$u'(L) = 0$ from 'cheby'	−2.111	−21.058	1.6978	6.0052	104.3914	−28.6972
$u'(L) = 0$ from '`bvp4c`'	−2.111	−21.058	1.6978	6.0052	104.3913	−28.6972
$u(\infty) = 0$	−2.6868	−406.7105	16.6004	3.0156	40.462	−14.8724

Table D3. Comparison of the bilinear forms for K_{ij}'s and J_{ij}'s by using different boundary conditions. This is for the case $d = 4$.

Boundary conditions	K_{11}	K_{22}	K_{12}	J_{11}	J_{22}	J_{12}
In [10, pp 7-8], $u'(L) = 0$	−8.0178	−31.8102	4.6472	147	3404	−728
$u'(L) = 0$ from 'cheby'	−8.0169	−32.0677	4.6791	158.4112	3764.4032	−792.1838
$u'(L) = 0$ from '`bvp4c`'	−8.0169	−32.0677	4.6791	158.4114	3764.4103	−792.1853
$u(\infty) = 0$	−8.0401	−159.7802	2.9583	13.4391	200.4192	−73.3805

$$\mathbf{MP} - \mathbf{f}(\mathbf{P}) = \mathbf{0}, \tag{C.7}$$

with the first and last rows substituted by the prescribed boundary conditions. This system (C.7) can be solved, for example, by the matlab solver '`fsolve`'.

Figure C1 shows the comparison of the profiles for V_2 when $d = 8$ and $r \gg 1$. Table C1 shows the difference of the ground state Q and $P\mathrm{e}^{-r}$, as well as the difference of V_2 calculated from Q and P, denoted by V_2 and $\tilde{V}_2$ correspondingly. Note how this method allows us to describe the 'exponential' decay and completely avoid oscillations!

Appendix D. Comparison with prior results on the spectral property in $d = 2, 3, 4$

In this part we list our numerical results for $d = 2, 3, 4$ to confirm that we get similar results as the ones in Fibich, Merle and Raphaël [10]. One can see that while the different boundary conditions, $u'(L) = 0$ and $u(\infty) = 0$, generate the different outcomes, this does not affect the proof of the spectral property 1 in those dimensions, as the signs of the quantities under consideration remain the same, see tables D1–D3. We do see some differences between our results and the results in [10], even when using the same boundary condition (however, this

Table D4. Comparison of the bilinear forms for K_{11}'s and J_{11}'s with the results from [29] obtained by '`bvp4c`', here, $L_2Z_1 = Q + rQ_r$ and $J_{11} = \langle L_2Z_1, Z_1\rangle$. This is for the 3D cubic NLS equation (L^2-supercritical).

3D cubic case	K_{11}	J_{11}
Numerical results in [29, p 14]	1.048 46	−0.662 038
Our numerical results by 'cheby'	1.048 46	−0.662 038

does not influence the outcome for the spectral property 1). Note that the situation is different in dimension five (and higher) as we discussed in the paper.

To further justify our numerical results, we also studied the (L^2-supercritical) 3D cubic NLS equation ($d = 3$ and $p = 3$), which was discussed by Marzuola and Simpson in [29]. From table D4, one can see that our numerical results match the results of Marzuola and Simpson [29] very well.

ORCID iDs

Svetlana Roudenko https://orcid.org/0000-0002-7407-7639

References

[1] Akrivis G D, Dougalis V A, Karakashian O A and McKinney W R 2003 Numerical approximation of blow-up of radially symmetric solutions of the nonlinear Schrödinger equation *SIAM J. Sci. Comput.* **25** 186–212
[2] Akrivis G D, Dougalis V A, Karakashian O A and McKinney W R 1993 Galerkin-finite element methods for the nonlinear Schrödinger equation *Advances on Computer Mathematics and its Applications* ed E Lipitakis (Singapore: World Scientific) pp 85–106
[3] Birem M and Klein C 2016 Multidomain spectral method for Schrödinger equations *Adv. Comput. Math.* **42** 395–423
[4] Berestycki H and Lions P 1983 Nonlinear scalar field equations. I. Existence of a ground state *Arch. Ration. Mech. Anal.* **82** 313–45
[5] Budneva V, Synakh V and Zakharov V 1975 Certain modes for wave collapse *Sov. J. Plasma Phys.* **1** 335–8
[6] Buslaev V S and Perelman G S 1992 Nonlinear scattering: the states which are close to a soliton *Zap. Nauchn. Sem. POMI* **200** 38–50
[7] Cazenave T 2003 *Semilinear Schrödinger Equations* (Providence, RI: American Mathematical Society)
[8] Dyachenko S, Newell A and Zakharov V 1992 Optical turbulence: weak turbulence, condensates and collapsing filaments in the nonlinear Schrödinger equation *Physica* D **57** 96–160
[9] Fibich G 2015 *The Nonlinear Schrödinger Equation, Singular Solutions and Optical Collapse* (Berlin: Springer)
[10] Fibich G, Merle F and Raphaël P 2006 Proof of a spectral property related to the singularity formation for the L^2 critical nonlinear Schrödinger equation *Physica* D **220** 1–13
[11] Fibich G, Merle F and Raphaël P 2017 Erratum to 'Proof of a spectral property related to the singularity formation for the L^2 critical nonlinear Schrödinger equation' (private communication)
[12] Fibich G and Papanicolaou G 1999 Self-focusing in the perturbed and unperturbed nonlinear Schrödinger equation in critical dimension *SIAM J. Appl. Math.* **60** 183–240
[13] Fraiman G M 1985 Asymptotic stability of manifold of self-similar solutions in self-focusing *Sov. Phys.—JETP* **61** 228–33
Fraiman G M 1985 Asymptotic stability of manifold of self-similar solutions in self-focusing *Zh. Éksper. Teoret. Fiz.* **88** 390–400 (translated from Russian)
[14] Ginibre J and Velo G 1979 On a class of nonlinear Schrödinger equations I. The Cauchy problem, general case *J. Funct. Anal.* **32** 1–32

[15] Glassey R 1977 On the blowing up of solutions to the Cauchy problem for nonlinear Schrödinger equation *J. Math. Phys.* **18** 1794–7
[16] Goldman M, Rypdal K and Hafizi B 1980 Dimensionality and dissipation in Langmuir collapse *Phys. Fluids* **23** 945–55
[17] Holmer J, Platte R and Roudenko S 2010 Blow-up criteria for the 3D cubic NLS equation *Nonlinearity* **23** 977–1030
[18] Holmer J and Roudenko S 2012 Blow-up solutions on a sphere for the 3D quintic NLS in the energy space *Anal. PDE* **5** 475–512
[19] Holmer J and Roudenko S 2011 A class of solutions to the 3D cubic nonlinear Schrödinger equation that blow-up on a circle *AMRX Appl. Math. Res. Express* **2011** 23–94
[20] Holmer J and Roudenko S 2007 On blow-up solutions to the 3D cubic nonlinear Schrödinger equation *AMRX Appl. Math. Res. Express* **1** abm004
[21] Kosmatov N E, Shvets V F and Zakharov V E 1991 Computer simulation of wave collapses in the nonlinear Schrödinger equation *Physica* D **52** 16–35
[22] Kwong M K 1989 Uniqueness of positive solutions of $\Delta u - u + u^p = 0$ in $\mathbb{R}^n$ *Arch. Ration. Mech. Anal.* **105** 243–66
[23] Landman M J, LeMesurier B, Papanicolaou G, Sulem C and Sulem P-L 2005 *Singular Solutions of the Cubic Schrödinger Equation, 'Integrable Systems and Applications'* (*Lecture Notes in Physics* vol 342) (Berlin: Springer) pp 207–17
[24] Landman M J, Papanicolaou G, Sulem C and Sulem P-L 1988 Rate of blowup for solutions of the nonlinear Schrödinger equation at critical dimension *Phys. Rev.* A **38** 3837–43
[25] Landman M J, Papanicolaou G, Sulem C, Sulem P-L and Wang X 1988 Stability of isotropic singularities for the nonlinear Schrödinger equation *Phys. Rev.* A **38** 3837–43
[26] LeMesurier B, Papanicolaou G, Sulem C and Sulem P-L 1988 Local structure of the self-focusing singularity of the nonlinear Schrödinger equation *Physica* D **32** 210–26
[27] Lushnikov P M, Dyachenko S A and Vladimirova N 2013 Beyond leading-order logarithmic scaling in the catastrophic self-focusing of a laser beam in Kerr media *Phys. Rev.* A **88** 13–845
[28] Malkin V M 1993 On the analytical theory for stationary self-focusing of radiation *Physica* D **64** 251–66
[29] Marzuola J and Simpson G 2011 Spectral analysis for matrix Hamiltonian operators *Nonlinearity* **24** 389–429
[30] McLaughlin D, Papanicoaou G, Sulem C and Sulem P-L 1986 Focusing singularity of the cubic Schrödinger equation *Phys. Rev.* A **34** 1200–10
[31] Merle F 1992 On uniqueness and continuation properties after blow-up time of self-similar solutions of nonlinear Schrödinger equation with critical exponent and critical mass *Commun. Pure Appl. Math.* **45** 203–54
[32] Merle F 1993 Determination of blow-up solutions with minimal mass for nonlinear Schrödinger equations with critical power *Duke Math. J.* **69** 427–54
[33] Merle F and Raphaël P 2005 Blow up dynamic and upper bound on the blow up rate for critical nonlinear Schrödinger equation *Ann. Math.* **161** 157–222
[34] Merle F and Raphaël P 2003 Sharp upper bound on the blow up rate for critical nonlinear Schrödinger equation *Geom. Funct. Anal.* **13** 591–642
[35] Merle F and Raphaël P 2004 On universality of blow up profile for L^2 critical nonlinear Schrödinger equation *Inventiones Math.* **156** 565–672
[36] Merle F and Raphaël P 2006 Sharp lower bound on the blow up rate for critical nonlinear Schrödinger equation *J. Am. Math. Soc.* **19** 37–90
[37] Perelman G 2001 On the blow up phenomenon for the critical nonlinear Schrödinger equation in 1D *Ann. Henri Poincaré* **2** 605–73
[38] Perelman G 2000 On the blow up phenomenon for the critical nonlinear Schrödinger equation in 1D *Séminaire: Équations aux Dérivées Partielles Polytechnique* **1999-2000** 1–14
[39] Raphaël P 2005 Stability of the log–log bound for blow up solutions to the critical nonlinear Schrödinger equation *Math. Ann.* **331** 577–609
[40] Reed M and Simon B 1978 *Method of Modern Mathematical Physics IV. Analysis of Operators* (London: Academic)
[41] Rypdal K and Rasmussen J 1986 Blow-up in nonlinear Schrödinger equations II *Phys. Scr.* **33** 498–504

[42] Simpson G and Zwiers I 2011 Vortex collapse for the L -critical nonlinear Schrödinger equation *J. Math. Phys.* **52** 83–503
[43] Shen J, Tang T and Wang L 2015 *Spectral Method, Algorithms, Analysis and Applications* (Berlin: Springer)
[44] Sulem C and Sulem P-L 1999 *The Nonlinear Schrödinger Equation. Self-Focusing and Wave-Collapse* (Berlin: Springer)
[45] Sulem P-L, Sulem C and Patera A 1984 Numerical simulation of singular solutions of the two-dimensional cubic Schrödinger equation *Commun. Pure Appl. Math.* **37** 755–78
[46] Synakh V and Zakharov V 1975 The nature of the self-focusing singularity *Sov. Phys.—JETP* **41** 465–8
[47] Titchmarsh E C 1946 *Eigenfunction Expansions Associated with Second-Order Differential Equations* (Oxford: Clarendon)
[48] Trefethen L N 2000 *Spectral Method in Matlab* (Philadelphia, PA: SIAM)
[49] Vlasov S N, Petrishchev V A and Talanov V I 1971 Averaged description of wave beams in linear and nonlinear media (the method of moments) *Radiophysics Quantum Electron.* **14** 1062–70
Vlasov S N, Petrishchev V A and Talanov V I 1971 Averaged description of wave beams in linear and nonlinear media (the method of moments) *Radiofizika* **14** 1353–63 (translated from Izvestiya Vysshikh Uchebnykh Zavedenii)
[50] Vlasov S N, Piskunova L V and Talanov V I 1978 Structure of the field near a signularity arising from self-focusing in a cubically nonlinear medium *Sov. Phys.—JETP* **48** 808–12
[51] Weinstein M I 1983 Nonlinear Schrödinger equations and sharp interpolation estimates *Commun. Math. Phys.* **87** 567–76
[52] Weinstein M I 1986 Lyapunov stability of ground states of nonlinear dispersive evolution equations *Commun. Pure Appl. Math.* **39** 51–68
[53] Wood D 1984 The self-focusing singularity in the nonlinear Schrödinger equation *Stud. Appl. Math.* **71** 103–15
[54] Kai Yang Formation of singularities in nonlinear dispersive PDE, Pro-Quest LLC 2018 *PhD Thesis* The George Washington University
[55] Zakharov V E 1972 Collapse of Langmuir waves *Zh. Eksp. Teor. Fiz.* **62** 1745–51
Zakharov V E 1972 Collapse of Langmuir waves *Sov. Phys.—JETP* **35** 908–14 (Engl. transl.)